ESAIM: M2AN 59 (2025) 201–230
https://doi.org/10.1051/m2an/2024078

ESAIM: Mathematical Modelling and Numerical Analysis
www.esaim-m2an.org

REDUCED BASIS METHOD FOR THE ELASTIC SCATTERING BY MULTIPLE SHAPE-PARAMETRIC OPEN ARCS IN TWO DIMENSIONS

José Pinto[1] and Fernando Henríquez[2,*]

Abstract. We consider the elastic scattering problem by multiple disjoint arcs or *cracks* in two spatial dimensions. A key aspect of our approach lies in the parametric description of each arc's shape, which is controlled by a potentially high-dimensional, possibly countably infinite, set of parameters. We are interested in the efficient approximation of the parameter-to-solution map employing model order reduction techniques, specifically the reduced basis method. Firstly, we use boundary potentials to transform the boundary value problem, originally posed in an unbounded domain, into a system of boundary integral equations set on the parametrically defined open arcs. We adopt the two-phase paradigm (offline and online) of the reduced basis method to construct a fast surrogate. In the offline phase, we construct a reduced order basis tailored to the single arc problem assuming a complete decoupling among arcs. In the online phase, when computing solutions for the multiple arc problem with a new parametric input, we use the aforementioned basis for each individual arc. We present a comprehensive theoretical analysis of the method, fundamentally based on our previous work [Pinto *et al.*, *J. Fourier Anal. Appl.* **30** (2024) 14]. In particular, the results stated therein allow us to find appropriate bounds for the so-called Kolmogorov width. Finally, we present a series of numerical experiments demonstrating the advantages of our proposed method in terms of both accuracy and computational efficiency.

Mathematics Subject Classification. 35J05, 65R20, 65N38.

Received March 16, 2024. Accepted October 28, 2024.

1. Introduction

Solving parametric partial differential equations (pPDEs) is a common task in many areas of science and engineering. Parameters are used to describe various aspects of a mathematical model, such as material properties or variations in the problem's physical domain. Traditionally, methods like Finite Differences, Finite Volumes, and Finite Elements have been employed to numerically solve these problems. However, applications involving multiple-query or real-time problems require repeated and rapid evaluations of the high-fidelity or full-order model for different parametric inputs. This quickly becomes computationally intractable, making complexity reduction methods in the parameter space necessary for efficient handling of these models.

Keywords and phrases. Model order reduction, reduced basis method, boundary element method, open arcs.

[1] Facultad de Ingeniería y Ciencias, Universidad Adolfo Ibáñez, Santiago, Chile.

[2] Chair of Computational Mathematics and Simulation Science (MCSS), École Polytechnique Fédéral de Lausanne, Lausanne, Switzerland.

*Corresponding author: fernando.henriquez@asc.tuwien.ac.at

The Reduced Basis (RB) method aims to accelerate the computation of the solution of pPDEs by using a two-stage paradigm. First, in an *offline* phase, a collection of so-called *snapshots* or high-fidelity solutions of the problem are computed for a set of parametric inputs. Then, a reduced-dimensional basis is constructed using these collection of solutions. Currently, two main approaches are used: POD [33] and greedy strategies [5,6,18,28]. POD establishes a set of samples in the parameter space in advance, calculating the corresponding high-fidelity solutions. A reduced basis is then computed using the Singular Value Decomposition (SVD) of the snapshot matrix. Conversely, greedy strategies sequentially add new elements to the basis in such a way that each new element provides the best possible improvement in approximating the *solution manifold*. Once the reduced basis is constructed using either method, the original high-fidelity problem is projected onto this basis, marking the *online* phase of the RB method. For further details, we refer the reader to [29,38–40].

Constructing reduced spaces for time-independent problems becomes a computational challenge, particularly when the parameter space is of high, potentially infinite, dimension. Efficiently approximating maps with high-dimensional parametric inputs presents major challenges to traditional computational methods due to the so-called *curse of dimensionality* in the parameter space. In [11], polynomial surrogates of high-dimensional input maps are shown to converge independently of dimension, provided there is an *holomorphic* dependence on the parametric input. Computationally, this property, often referred to as parametric holomorphy, underpins provably dimension-independent convergence rates for a variety of methods including, for instance, Smolyak interpolation and quadrature [42,44] and high-order Quasi-Monte Carlo integration (HoQMC) [19,21] among others. In particular, in the context of model order reduction and the RB method, parametric holomorphy guarantees dimension-independent bounds for Kolmogorov's width [12,13], leading to dimension-independent convergence rates for both the POD-based and greedy strategies [3,5,8–10,34]. Furthermore, in the multiple-arc setting under consideration in this work, the decay of Kolmogorov's width becomes slower as the number of arcs increases, adding to the difficulty posed by the high dimensionality of the parameter space.

In the context of shape-parametric Boundary Integral Operators (BIOs), one may find a variety of works addressing and proving the aforementioned parametric holomorphy property. In [25,26], the holomorphic dependence of the Calder'on projector on boundaries of class $\mathcal{C}^2$ has been established. Furthermore, in [15–17], analytic shape differentiability of BIOs has been studied for problems in two and three dimensions. In [22], parametric holomorphy of the combined integral operator has been proved for piecewise $\mathcal{C}^2$-boundaries, thus allowing polygonal/polyhedral boundaries. However, relevant to this work is [37], which addresses the case of multiple open arcs in two dimensions.

1.1. Contributions

In this work, we perform model order reduction for the elastic scattering problem by multiple shape-parametric open arcs. Firstly, as in [1,2,7,30,32,43], we cast the original boundary value problem as an equivalent system of boundary integral equations (BIEs) posed on the collection of open arcs. Then, following the approach presented in [23], we propose and thoroughly analyze a reduced basis method for this shape-parametric formulation.

A key insight of this method lies in the construction of a reduced basis for each shape-parametric arc, which is then used as a building block for the complexity reduction of the multiple interacting arcs configuration. For the numerical approximation of the high-fidelity solution, we use a custom spectral Galerkin Boundary Element (BE) implementation tailored to handle the problem's characteristic singular nature at the arcs' endpoints.

We provide a comprehensive convergence analysis that accounts for discretization in the parameter space, the BE discretization, and parametric dimension truncation. Unlike previous works in this field, we also provide a systematic analysis for constructing the RB space for elastic scattering by multiple arcs using the single arc problem as a building block. These insights are supported by a series of numerical experiments. Indeed, our computational results show that the multiple arcs problem cannot be efficiently reduced using standard procedures. However, the construction based on the single arc problem leads to a more efficient algorithm.

1.2. Outline

This work is structured as follows. In Section 2, we introduce notation and relevant technical results to be used throughout this work. Section 3 introduces the elastic scattering problem by multiple open arcs, together with its boundary integral formulation and details of the spectral Galerkin BE discretization. Next, in Section 4 we introduce the reduced basis method for pPDES. Particular emphasis is given to the construction of a reduced order model for the multiple arc problem by taking as starting point a reduced basis constructed for a single arc. In Section 5 we provide a complete analysis of the reduced order method for the multiple arc problem. Finally, in Section 6 we present numerical experiments portraying the performance of the reduced basis approach, whereas in Section 7 we provide final concluding remarks.

2. Preliminaries

2.1. Notation

Throughout, vectors are indicated by boldface symbols. For any $\boldsymbol{v} \in \mathbb{C}^n$, with $n \in \mathbb{N}$, we consider the Euclidean norm $\|\boldsymbol{v}\| = \sqrt{\boldsymbol{v} \cdot \overline{\boldsymbol{v}}}$. In $\mathbb{R}^2$, we denote by $\boldsymbol{e}_1 = (1,0)^\top$, $\boldsymbol{e}_2 = (0,1)^\top$ the canonical vectors. Given an angle $\theta \in [0, 2\pi)$, the corresponding directional vector is $\boldsymbol{e}_{(\theta)} = (\cos\theta, \sin\theta)^\top$. The rotation matrix associated with the angle θ is

$$\boldsymbol{R}_\theta = \begin{pmatrix} \cos\theta & -\sin\theta \\ \sin\theta & \cos\theta \end{pmatrix}, \tag{2.1}$$

thus we have that $\boldsymbol{e}_{(\theta)} = \boldsymbol{R}_\theta \boldsymbol{e}_1$.

Given real numbers a, b, we say that $a \lesssim b$ if there exists a positive constant c, independent of the variables relevant to the corresponding analysis, such that $a \leq cb$. If $a \lesssim b$ and $b \lesssim a$ we write $a \cong b$.

Let X be a Banach space. Its anti-dual is denoted by $X^\star$, and the evaluation of an element $f \in X^\star$ on an element $x \in X$ is denoted by $\langle f, x \rangle$. Given another Banach space Y, we denote by $\mathcal{L}(X, Y)$ the space of bounded linear operators from X to Y. As it is customary, we equip it with the standard operator norm, thus rendering it a Banach space itself.

Given a Hilbert space H and a closed subspace $V \subset H$, we denote the corresponding orthogonal projection by P_V^H, or simply P_V when the space H is clear from the context.

2.2. Functional spaces

First, let us recall the definition of Hölder spaces. Given two non-empty, open and connected sets $\Omega_1 \subset \mathbb{R}^{d_1}, \Omega_2 \subset \mathbb{R}^{d_2}$, for $d_1, d_2 \in \mathbb{N}$, the space $\mathcal{C}^{m,\alpha}(\Omega_1, \Omega_2)$ consists of functions $f : \Omega_1 \to \Omega_2$ with derivatives up to order m in Ω_1, each of them continuous over $\overline{\Omega_1}$, and such that the derivatives of order m fulfils the α-Hölder continuous condition, *i.e.* $\|g(\mathbf{x}) - g(\mathbf{y})\| \lesssim \|\mathbf{x} - \mathbf{y}\|^\alpha$ with g being any derivative of total order up to and including m of f.

In order to describe the relevant geometries we will make use of a subset of $\mathcal{C}^{m,\alpha}\big((-1,1), \mathbb{R}^2\big)$, denoted by $\mathcal{C}_b^{m,\alpha}\big((-1,1), \mathbb{R}^2\big)$ consisting of all $\boldsymbol{r} \in \mathcal{C}^{m,\alpha}\big((-1,1), \mathbb{R}^2\big)$ such that $\|\boldsymbol{r}'(t)\| > 0$, $t \in (-1,1)$, and having a globally defined inverse, *i.e.* $\boldsymbol{r} : (-1,1) \to \mathbb{R}^2$ has a unique inverse.

We also introduce the functional spaces used to properly state the elastic scattering problem on cracks. Set $w(t) = \sqrt{1-t^2}$, $t \in (-1,1)$. We denote by $T_n(t)$ the nth Chebyshev polynomial of the first kind normalized according to

$$\int_{-1}^{1} T_m(t) T_l(t) w^{-1}(t)\, \mathrm{d}t = \delta_{m,l}, \quad l, m \in \mathbb{N}_0,$$

where $\delta_{l,m} = 1$ if $l = m$ and $\delta_{l,m} = 0$ if $l \neq m$. For a smooth function $u : [-1,1] \to \mathbb{C}$ we define two sequences of Chebyshev coefficients as

$$u_n \coloneqq \int_{-1}^{1} u(t) T_n(t)\, \mathrm{d}t \quad \text{and} \quad \widehat{u}_n \coloneqq \int_{-1}^{1} u(t) T_n(t) w^{-1}(t)\, \mathrm{d}t, \quad n \in \mathbb{N}_0.$$

By using a duality argument, these definitions are extended to distributions, and we define the following spaces: For $s \in \mathbb{R}$ we set

$$T^s := \left\{ u : \|u\|_{T^s}^2 = \sum_{n=0}^{\infty} (1+n^2)^s |u_n|^2 < \infty \right\},$$
$$W^s := \left\{ u : \|u\|_{W^s}^2 = \sum_{n=0}^{\infty} (1+n^2)^s |\widehat{u}_n|^2 < \infty \right\}.$$

The dual space of T^s can be identified with W^{-s}, where the duality product, that subsequently is denoted as $\langle \cdot, \cdot \rangle$, is the extension of the $L^2((-1,1))$ inner product without any weight function. Throughout this work we assume that this identification has been made.

For certain values of s, these spaces coincide with standard Sobolev spaces in the interval $(-1,1)$. In fact, we have that

$$T^{-\frac{1}{2}} = \widetilde{H}^{-\frac{1}{2}}((-1,1)) \quad \text{and} \quad W^{\frac{1}{2}} = H^{\frac{1}{2}}((-1,1)).$$

We refer the reader to Chapter 3 from [35], for the classical definition of Sobolev spaces of integer and fractional orders.

Finally, for $s \in \mathbb{N}$, we define the following product spaces

$$\mathbb{T}^s = T^s \times T^s \quad \text{and} \quad \mathbb{W}^s = W^s \times W^s.$$

These will be extensively used in the next sections.

2.3. Problem geometry

We provide a precise description of the type of open arcs to be considered in the rest of this work. We uniquely identify each open arc with one of its corresponding parametrizations. Each open arc is described as a function from $[-1,1]$ with values $\mathbb{R}^2$ satisfying the following properties:

(i) The function is an element of $\mathcal{C}^{m,\alpha}((-1,1);\mathbb{R}^2)$, with $m \in \mathbb{N}$, $\alpha \in [0,1]$, and $m + \alpha > 2$.
(ii) The derivative of the function, *i.e.* the tangent vector, is nowhere null. Therefore, it belongs to $\mathcal{C}_b^{m,\alpha}\big((-1,1),\mathbb{R}^2\big)$.

The latter requirement implies that the parametrization function is invertible. In the following we set $\mathrm{U} := \left[-\frac{1}{2},\frac{1}{2}\right]^{\mathbb{N}}$. Of special interest will be collection of open arcs that are determined by a parametric input $\boldsymbol{y} \in \mathrm{U}$ of the form

$$\boldsymbol{r}(\boldsymbol{y},t) = \boldsymbol{r}_0(t) + \sum_{n=1}^{\infty} y_n \boldsymbol{r}_n(t), \tag{2.2}$$

here $\boldsymbol{r}_0$ is an open arc with a nowhere null tangent vector, and in the following we refer to it as the *reference* arc. In the following, for each $\boldsymbol{y} \in \mathrm{U}$, when referring to an open arc as an element of $\mathcal{C}^{m,\alpha}((-1,1);\mathbb{R}^2)$ we use the notation $\boldsymbol{r}(\boldsymbol{y})$. In contrast, when referring to a point in $\mathbb{R}^2$ described by the arc's parametrization we use the notation $\boldsymbol{r}(\boldsymbol{y},t)$ for some $t \in [-1,1]$. The set $\{\boldsymbol{r}_n\}_{n\in\mathbb{N}}$ is a subset of $\mathcal{C}^{m,\alpha}((-1,1),\mathbb{R}^2)$ and we will refer to it as the perturbation basis. In order to ensure that for any value of the parameter $\boldsymbol{y}$ the parametrization $\boldsymbol{r}(\boldsymbol{y})$ as in (2.2) is indeed an open arc in $\mathbb{R}^2$, we work under the following assumptions.

Assumption 2.1. (1) *The perturbation basis $\boldsymbol{r}_n$ is such that, $\boldsymbol{b} = \left\{\|\boldsymbol{r}_n\|_{\mathcal{C}^{m,\alpha}((-1,1);\mathbb{R}^2)}\right\}_{n\in\mathbb{N}}$, $n \in \mathbb{N}$, is a sequence in $\ell^p(\mathbb{N})$ for some $p \in (0,1)$.*

(2) *There exists $\zeta \in (0,1)$ such that*

$$\sup_{t\in(-1,1)} \sum_{n=1}^{\infty} \|(\boldsymbol{r}_n)'(t)\| \leq \zeta \inf_{t\in(-1,1)} \|(\boldsymbol{r}_0)'(t)\|.$$

Under these conditions for $\boldsymbol{r}_0$ and $\{b_n\}_{n\in\mathbb{N}}$, and using the mean value theorem we can ensure that $\boldsymbol{r}(\boldsymbol{y})$ is an open arc for any $\boldsymbol{y}\in \mathrm{U}$.

As we are interested in the multiple arc problem, we also consider M parametrically defined collections of open arcs, each of them of the form (2.2). We denote these families by $\boldsymbol{r}^1(\boldsymbol{y}^1),\dots,\boldsymbol{r}^M(\boldsymbol{y}^M)$, each of them having their corresponding reference arc denoted by $\boldsymbol{r}_0^1,\dots \boldsymbol{r}_0^M$, while the perturbations basis would be assumed to be the same for any of the M collections.

We further assume that fixed parts are line segments of the form

$$\boldsymbol{r}_0^j(t)=\boldsymbol{c}_j+\varrho_j(\cos\varphi_j,\sin\varphi_j)^\top t,\quad t\in(-1,1),\quad j=1,\dots,M$$

where $\boldsymbol{c}_j\in[-B,B]\times[-B,B]$, for some $B>0$, is the arc's center. The length of the segment is $\varrho_j\in[r_{\min},r_{\max}]$, for given $0<r_{\min}<r_{\max}$, while $\varphi_j\in[0,\pi)$ defines the orientation of the segment.

We also assume that there exist $d_{\min},d_{\max}$, with $0<d_{\min}<d_{\max}$, such that $d_{\min}\le\|\boldsymbol{c}_k-\boldsymbol{c}_j\|\le d_{\max}$, for $k\neq j$, and that

$$d_{\min}>2\left(r_{\max}+\sum_{n=1}^{\infty}\sup_{t\in[-1,1]}\|\boldsymbol{r}_n(t)\|\right).$$

This last condition ensures that the arcs are pairwise disjoint.

3. Elastic wave scattering by multiple open arcs

In this section, we introduce the elastic scattering problem by multiple open arcs together with its spectral BE Galerkin discretization using weighted polynomials. We refer to [31] and references therein for more details on these aspects of the problem.

3.1. Problem formulation

Given $\kappa\in\mathbb{R}$, $\theta\in[0,2\pi)$ we denote a scalar plane wave with incidence angle θ and wave-number κ by

$$g_{\theta,\kappa}(\boldsymbol{x})=\exp\big(\imath\kappa\boldsymbol{e}_{(\theta)}\cdot\boldsymbol{x}\big),$$

where we recall that $\boldsymbol{e}_{(\theta)}=(\cos\theta,\sin\theta)^\top$. Let us consider M families of parameterized open arcs as in Section 2.3, whose image in $\mathbb{R}^2$ are denoted by $\Gamma(\boldsymbol{y}^1,\dots,\boldsymbol{y}^M)$. We fix a direction $\theta_0\in[0,2\pi)$ that corresponds to that of the incoming plane-wave. In addition, we also fix ω as the the problem's frequency, and we denote by λ,μ the Lamé parameters. Then, for a given realization of the parameters $\boldsymbol{y}^1,\dots,\boldsymbol{y}^M$, we seek $\boldsymbol{U}:\mathbb{R}^2\to\mathbb{C}^2$ such that

$$\begin{aligned}(\mu\Delta+(\lambda+\mu)\nabla\nabla\cdot)\boldsymbol{U}+\omega^2\boldsymbol{U}=0\quad&\text{in}\quad\mathbb{R}^2\setminus\overline{\Gamma(\boldsymbol{y}^1,\dots,\boldsymbol{y}^M)},\\ \boldsymbol{U}=\boldsymbol{e}_{(\theta_0)}g_{\theta_0\kappa_{\mathsf{p}}},\quad&\text{on }\Gamma(\boldsymbol{y}^1,\dots,\boldsymbol{y}^M)\\ &+\text{Condition at infinity},\end{aligned}$$

where $\kappa_{\mathsf{p}}=\sqrt{\frac{\omega}{\lambda+2\mu}}$, and the radiation condition at infinity is the standard Kupradze's one.

Using standard arguments of boundary integral formulations ([35], Chap. 7) we look for a solution of the form[1]

$$\boldsymbol{U}(\mathbf{x})=\sum_{j=1}^{M}\int_{-1}^{1}\mathbf{G}(\mathbf{x},\boldsymbol{r}^j(\boldsymbol{y}^j,\tau))\boldsymbol{u}^j(\boldsymbol{y}^1,\dots,\boldsymbol{y}^M,\tau)\,\mathrm{d}\tau,\quad\mathbf{x}\in\mathbb{R}^2\setminus\overline{\Gamma(\boldsymbol{y}^1,\dots,\boldsymbol{y}^M)},\tag{3.1}$$

where $\mathbf{G}$ is the fundamental solution to the elastic wave operator[2], and $\boldsymbol{u}^j(\boldsymbol{y}^1,\dots,\boldsymbol{y}^M,\cdot)$ are unknown densities defined in $(-1,1)$, for $j=1,\dots,M$. By imposing the boundary conditions on the representation formula stated in

[1]From standard boundary integral potentials properties this representation formula is continuous across $\Gamma(\boldsymbol{y}^1,\dots,\boldsymbol{y}^M)$.

[2]The fundamental solution depends on the parameters ω,λ,μ, however as these are fixed for each instance of the problem we do not incorporate them in the notation.

(3.1) we obtain the following system of boundary integral equations for the unknown densities $\boldsymbol{u}^j(\boldsymbol{y}^1,\dots,\boldsymbol{y}^M,\cdot)$, for $j=1,\dots,M$:

$$\sum_{j=1}^{M} \boldsymbol{V}_{\boldsymbol{r}^k(\boldsymbol{y}^k),\boldsymbol{r}^j(\boldsymbol{y}^j)}\boldsymbol{u}^j(\boldsymbol{y}^1,\dots,\boldsymbol{y}^M,\cdot)(t)=\boldsymbol{g}_k(t),\quad k=1,\dots,M, \tag{3.2}$$

where the weakly singular operator $\boldsymbol{V}_{\boldsymbol{r},\boldsymbol{p}}$ is defined, for a pair of open arcs $\boldsymbol{r},\boldsymbol{p}$ and a density function $\boldsymbol{u}$, as

$$\boldsymbol{V}_{\boldsymbol{r},\boldsymbol{p}}\boldsymbol{u}(t)=\int_{-1}^{1}\mathbf{G}(\boldsymbol{r}(t),\boldsymbol{p}(\tau))\boldsymbol{u}(\tau)\,\mathrm{d}\tau$$

and the right-hand side is given by

$$\boldsymbol{g}_k(t)=\boldsymbol{e}_{(\theta_0)}g_{\theta_0,\kappa_p}(\boldsymbol{r}^k(\boldsymbol{y}^k,t)). \tag{3.3}$$

We refer to [4] for the functional setting and well-posedness of (3.2).

3.2. High-fidelity discretization

We now provide the construction of the spectral BE Galerkin discretization of (3.2) used as the high-fidelity solver for the construction of the reduced basis method ahead in (4.2) To this end, we define the following families of finite dimensional spaces

$$T_N=\left\{u(t)=\sum_{n=0}^{N}a_nT_n(t)w^{-1}(t)\ \text{ with }\ \{a_n\}_{n=0}^{N}\subset\mathbb{C}\right\},\quad N\in\mathbb{N},$$

$$W_N=\left\{u(t)=\sum_{n=0}^{N}a_nT_n(t)\ \text{ with }\ \{a_n\}_{n=0}^{N}\subset\mathbb{C}\right\},\quad N\in\mathbb{N},$$

and set $\mathbb{T}_N=T_N\times T_N\subset\mathbb{T}^s$, $\mathbb{W}_N=W_N\times W_N\subset\mathbb{W}^s$, for $N\in\mathbb{N}$ and $s\in\mathbb{R}$. Having introduced these spaces, the discrete version of (3.2) reads as follows: For $\boldsymbol{y}^1,\dots,\boldsymbol{y}^M\in\mathrm{U}$, we seek $\boldsymbol{u}_N^j(\boldsymbol{y}^1,\dots,\boldsymbol{y}^M,\cdot)\in\mathbb{T}_N$, such that

$$\sum_{j=1}^{M}P_{\mathbb{W}_N}\boldsymbol{V}_{\boldsymbol{r}^k(\boldsymbol{y}^k),\boldsymbol{r}^j(\boldsymbol{y}^j)}\boldsymbol{u}_N^j(\boldsymbol{y}^1,\dots,\boldsymbol{y}^M,\cdot)(t)=P_{\mathbb{W}_N}\boldsymbol{g}_k(t),\quad k=1,\dots,M.$$

Using the following ansatz for the solution of (3.2)

$$\boldsymbol{u}_N^j(\boldsymbol{y}^1,\dots,\boldsymbol{y}^M,t)=\sum_{m=0}^{N}\sum_{p=1}^{2}\big(\boldsymbol{a}^{j,p}(\boldsymbol{y}^1,\dots,\boldsymbol{y}^M)\big)_m T_m(t)w(t)^{-1}\boldsymbol{e}_p,\quad t\in(-1,1),$$

we can write (3.2) as follows.

Problem 3.1. Given $N\in\mathbb{N}$ we seek $\boldsymbol{a}^{1,p}(\boldsymbol{y}^1,\dots,\boldsymbol{y}^M),\dots,\boldsymbol{a}^{M,p}(\boldsymbol{y}^1,\dots,\boldsymbol{y}^M)\in\mathbb{C}^{N+1}$, for $p\in\{1,2\}$, such that

$$\sum_{j=1}^{M}\mathbb{A}_{k,j}^{p,q}\boldsymbol{a}^{j,q}(\boldsymbol{y}^1,\dots,\boldsymbol{y}^M)=\boldsymbol{g}_{N,k}^{p},\quad k\in\{1,\dots,M\},\quad q\in\{1,2\},$$

where

$$\left(\mathbb{A}_{k,j}^{p,q}\right)_{\ell,m}=\left\langle\boldsymbol{V}_{\boldsymbol{r}^k(\boldsymbol{y}^k),\boldsymbol{r}^j(\boldsymbol{y}^j)}\frac{T_m}{w}\boldsymbol{e}_q,\frac{T_\ell}{w}\boldsymbol{e}_p\right\rangle,\quad \ell,m\in\{0,\dots,N\},\ p,q\in\{1,2\}$$

and

$$\left(\boldsymbol{g}_{N,k}^{p}\right)_\ell=\left\langle\boldsymbol{g}_k,\frac{T_l}{w}\boldsymbol{e}_p\right\rangle,\quad \ell\in\{0,\dots,N\},\ p\in\{1,2\}.$$

Remark 3.2. In [31] it was proven that if for a given realization of the parameters $\boldsymbol{y}^1, \dots, \boldsymbol{y}^M$ the resulting open arcs $\boldsymbol{r}^1(\boldsymbol{y}^1), \dots, \boldsymbol{r}^M(\boldsymbol{y}^M)$ are analytic, then asymptotically in N we obtain exponential convergence, *i.e.* there exist $\rho > 1$ and $N_0 \in \mathbb{N}$ such that for any $N \geq N_0$ it holds

$$\sum_{j=1}^{M} \|\boldsymbol{u}^j(\boldsymbol{y}^1, \dots, \boldsymbol{y}^M) - \boldsymbol{u}_N^j(\boldsymbol{y}^1, \dots, \boldsymbol{y}^M)\|_{\mathbb{T}^{-\frac{1}{2}}} \lesssim \rho^{-N},$$

where, in principle, the implicit constant depends on the parameters $\boldsymbol{y}^1, \dots, \boldsymbol{y}^M \in \mathrm{U}$.

3.2.1. Numerical implementation

We present an overview of some aspects concerning the computational implementation of the previously described spectral Galerkin BE discretzation, as these are important for the construction of the reduced model. We again refer to [30, 31] for some more details and improvements to the basic implementation.

For the implementation of the spectral Galerkin method we need to approximate two types of integrals:

$$\left\langle \boldsymbol{V}_{\boldsymbol{r}^k(\boldsymbol{y}^k), \boldsymbol{r}^j(\boldsymbol{y}^j)} \frac{T_m}{w} \boldsymbol{e}_q, \frac{T_l}{w} \boldsymbol{e}_p \right\rangle \quad \text{and} \quad \left\langle \boldsymbol{g}_k, \frac{T_l}{w} \boldsymbol{e}_p \right\rangle. \tag{3.4}$$

Let us start with the second type, which appears in the right-hand side of Problem 3.1. Since $\boldsymbol{g}_k$ is a smooth function we can simply compute these integrals using FFT. Concretely, we first construct the vector of evaluations

$$\mathfrak{g}_{\boldsymbol{k}} = (\boldsymbol{g}_k(x_j))_{j=0,\dots,N_c-1}, \quad x_j = \cos\left(\frac{\pi(N_c - 1 - j)}{N_c - 1}\right),$$

then we apply the discrete Fourier transform to this vector[3], and finally we perform an scaling as in [30]. The computational cost is of order $O(N \log N)$ per arc. Notice that we can think of the integration method as a linear function acting on vector of evaluations of the right-hand side.

Remark 3.3. While we do not provide all the details concerning the computation of these integrals, (we again refer to [30] for a detailed discussion), in a more abstract setting the computation of the integrals of the form

$$\left\langle f, \frac{T_l}{w} \right\rangle,$$

where f is a known function, can be thought as the application of a linear map L to the vector $\mathfrak{f} = f(x_j)_{j=0,\dots,N_c-1}$, where the points x_j are as in (3.4).

For the computation of the first type of terms in (3.4) we consider two separate cases. Firstly, for smooth component of the cross interaction between arcs, *i.e.* when $k \neq j$, we use a tensorization of the method applied to the right-hand side, with a cost of $O(N^2 \log N)$ operations.

Finally, the self-interaction case, *i.e.* $k = j$, is treated as in [31], thus it can be reduced to the computation of a regular integral (this is done as in the cross-interaction case), plus an integral of the form

$$I_{l,m} = \int_{-1}^{1} \int_{-1}^{1} \log|t - \tau| J(t, \tau) \frac{T_m}{w}(\tau) \frac{T_l}{w}(t) \, \mathrm{d}\tau \, \mathrm{d}t, \tag{3.5}$$

where J is an analytic function in both arguments. Using the exact same procedure used to treat the crossed interactions together with the orthogonality properties of Chebyshev polynomials, we can construct the approximation

$$J(t, s) \approx \sum_{p=0}^{Q} \sum_{q=0}^{Q} j_{p,q} T_p(t) T_q(s),$$

[3]The parameter N_c is selected according to a certain tolerance and at worst grows linearly with N.

with a computational cost of $O(Q^2 \log Q)$. On the other hand, from the well-known expansion

$$\log|t-s| = \sum_{n=0}^{\infty} d_n T_n(t) T_n(s),$$

using traditional Chebyshev properties we have that

$$I_{l,m} \approx \sum_{n=0}^{\infty} d_n (j_{l+n,m+n} + j_{l+n,|m-n|} + j_{|l-n|,m+n} + j_{|l-n|,|m-n|}), \tag{3.6}$$

where the error decays exponential with respect to Q, which is in turn proportional to N. The evaluation of (3.6) has a computational cost of $O(N^3)$. However, this could be reduced to $O(N^2 \log N)$ by using the convolution properties of the discrete Fourier transform. The total cost of assembling the linear system of equations is of order $O(M^2 N^2 \log N)$.

Remark 3.4. As in Remark 3.3, the algorithm for the computation of the matrix terms can be thought as linear function acting on evaluations of a kernel function. In the cross-interactions case the kernel function is the fundamental solution, while for the self-interactions we have two different linear functions, one acting on the evaluations of the function $J(t,s)$ as in (3.5)), and a second one, accounting for the regular part, which is the difference between the fundamental solution and $J(t,s)\log|t-s|$.

4. Model order reduction for multiple arcs

The high-fidelity discretization introduced in Section 3.2 provides a fast method to approximate the solution of the elastic scattering problem for a fixed geometry determined by the parameters $\boldsymbol{y}^1, \ldots, \boldsymbol{y}^M \in \mathrm{U}$. However, when aiming to solve this problem for a large number of parametric inputs, a new strategy is required, in particular as the number of arcs increases. To this end, we adopt a model order reduction perspective and resort to the reduced basis method.

This section is organized as follows: in Section 4.1, we revisit the fundamentals of the Galerkin Proper Orthogonal Decomposition (Galerkin-POD) approach, a well-established technique for constructing efficient reduced basis in the context of parametric problems. Subsequently, in Section 4.2, we outline a method for constructing an efficient Reduced Order Model (ROM) for configurations with multiple arcs. This approach involves building individual ROMs the single arc problem, and then use the same basis for the multiples arcs case.

To fully harness the benefits of the reduced basis approach one needs an efficient and fast way of constructing the high-fidelity problem projected in the reduced space. Even though we use an affine-parametric representation for each open arc, this does not translate into an affine decomposition of the underlying reduced problem. Following ideas introduced in [23] we apply the Empirical Interpolation Method (EIM) as described in Section 4.3 ahead.

4.1. Galerkin-POD and reduced order modelling

Let us briefly recall the Galerkin-POD method. Our presentation follows mainly Chapter 3 of [29] and Chapter 6 of [39].

For each $\boldsymbol{y} \in \mathrm{U}$, we seek $u(\boldsymbol{y}) \in X$ such that

$$\mathsf{a}(u(\boldsymbol{y}), v; \boldsymbol{y}) = \mathsf{g}(v, \boldsymbol{y}), \quad \forall v \in X, \tag{4.1}$$

where X is a Hilbert Space, for each $\boldsymbol{y} \in \mathbb{U}$, $\mathsf{a}(\cdot,\cdot;\boldsymbol{y}) : X \times X \to \mathbb{C}$ and $\mathsf{g}(\cdot;\boldsymbol{y}) \in X^\star$ denotes a parameter-dependent sesquilinear form and an anti-linear functional acting on X, respectively. We also define the solution manifold, *i.e.* the set all possible solutions to (4.1), as

$$\mathcal{M} \coloneqq \{u(\boldsymbol{y}) \in X : \ \boldsymbol{y} \in \mathrm{U}\} \subset X.$$

In addition, let $\{X_N\}_{N\in\mathbb{N}}$ be a family of finite-dimensional subspace of X, each one of dimension N, and let $\{\varphi_1,\dots,\varphi_N\}\subset X$ be a suitable basis of X_N, *i.e.* $X_N=\operatorname{span}\{\varphi_1,\dots,\varphi_N\}$. The Galerkin discretization of (4.1) reads: For each $\boldsymbol{y}\in\mathrm{U}$, we seek $u_N(\boldsymbol{y})\in X_N$, such that

$$\mathsf{a}(u_N(\boldsymbol{y}),v;\boldsymbol{y})=\mathsf{g}(v,\boldsymbol{y}),\quad \forall v\in X_N,$$

and we define the *discrete* solution manifold as

$$\mathcal{M}_N\coloneqq\{u_N(\boldsymbol{y})\in X_N:\ \boldsymbol{y}\in\mathrm{U}\}.$$

Equivalently, the Galerkin discretization of (4.1) using the following *anstaz*

$$u_N(\boldsymbol{y})=\sum_{j=1}^{N}(\boldsymbol{a}_N(\boldsymbol{y}))_j\varphi_j.$$

can be formulated as follows: For each $\boldsymbol{y}\in\mathrm{U}$ we seek $\boldsymbol{a}_N(\boldsymbol{y})\in\mathbb{C}^N$ such that

$$\mathbb{A}_N(\boldsymbol{y})\boldsymbol{a}_N(\boldsymbol{y})=\boldsymbol{g}_N(\boldsymbol{y}),$$

where for each $\boldsymbol{y}\in\mathrm{U}$

$$(\mathbb{A}_N(\boldsymbol{y}))_{i,j}=\mathsf{a}(\varphi_j,\varphi_i;\boldsymbol{y})\quad i,j=1,\dots,N\quad\text{and}\quad(\boldsymbol{g}_N(\boldsymbol{y}))_i=\mathsf{g}(\varphi_i;\boldsymbol{y})\quad i=1,\dots,N.$$

As we are working in a finite-dimensional space, it holds

$$\left\|\sum_{n=1}^{N}c_n\varphi_N\right\|_X^2\cong\sum_{n=1}^{N}|c_n|^2,$$

with a constant depending on X_N. Hence, the norm $\|\cdot\|_X$ in X_N and the vector 2-norm of the coefficients $\{c_n\}_{n=1}^N\in\mathbb{C}^N$ are equivalent with hidden constants depending of N.

For the construction of the reduced basis, we seek the subspace $V_R^{(\mathrm{rb})}$ of X_N of dimension $R<N$ solution to the following minimization problem

$$V_R^{(\mathrm{rb})}=\operatorname*{arg\,min}_{\substack{Z_R\subset X_N\\ \dim(Z_R)\le R}}\int_{\mathrm{U}}\|u_N(\boldsymbol{y})-\mathsf{P}_{Z_R}u_N(\boldsymbol{y})\|_X^2\,\mathrm{d}\boldsymbol{y}.\tag{4.2}$$

The above problem can be formulated using the algebraic form of the Galerkin discretization. The solution is given by a matrix $\mathbb{V}_R^{(\mathrm{rb})}\in\mathbb{C}^{N\times R}$ which is obtained by solving the following problem:

$$\mathbb{V}_R^{(\mathrm{rb})}=\operatorname*{arg\,min}_{\mathbb{W}\in\mathscr{V}_R}\int_{\mathrm{U}}\left\|\boldsymbol{a}(\boldsymbol{y})-\mathbb{W}\mathbb{W}^{\dagger}\boldsymbol{a}(\boldsymbol{y})\right\|^2\mathrm{d}\boldsymbol{y},\tag{4.3}$$

where $\mathscr{V}_R=\left\{\mathbb{W}\in\mathbb{C}^{N\times R}:\ \mathbb{W}^{\dagger}\mathbb{W}=\mathbb{I}_R\right\}$ and with $\mathbb{I}_R$ denoting the identity matrix of size $R\times R$.

While the solution of this problem is known (see, *e.g.* [39], Prop. 6.3), in practical implementations one considers a discretized version of the high-dimensional integral in (4.3). Provided a dimension truncation parameter $s\in\mathbb{N}$, we consider an equal weights, N_t-points quadrature rule in $\mathrm{U}^s=\left[-\frac{1}{2},\frac{1}{2}\right]^s$ with points $\{\boldsymbol{y}_1,\dots,\boldsymbol{y}_{N_t}\}\subset\mathrm{U}^s$. This yields the following approximation of (4.3):

$$\mathbb{V}_R^{(\mathrm{rb})}=\operatorname*{arg\,min}_{\mathbb{W}\in\mathscr{V}_R}\frac{1}{N_t}\sum_{j=1}^{N_t}\left\|\boldsymbol{a}(\boldsymbol{y}_j)-\mathbb{W}\mathbb{W}^{\dagger}\boldsymbol{a}(\boldsymbol{y}_j)\right\|^2.\tag{4.4}$$

The solution of this problem is given by the Schmidt–Eckart–Young theorem (see, *e.g.* [39], Prop. 6.1). Define the *snapshot* matrix

$$\mathbb{S} \coloneqq \big(\boldsymbol{a}(\boldsymbol{y}_1), \dots, \boldsymbol{a}(\boldsymbol{y}_{N_t})\big) \in \mathbb{C}^{N \times N_t}$$

and compute its SVD decomposition $\mathbb{S} = \mathbb{W}\Sigma\mathbb{Z}^\dagger$, where

$$\mathbb{W} = \big(\boldsymbol{w}_1, \dots, \boldsymbol{w}_N\big) \in \mathbb{C}^{N \times N} \quad \text{and} \quad \mathbb{Z} = \big(\boldsymbol{z}_1, \dots, \boldsymbol{z}_{N_t}\big) \in \mathbb{C}^{N_t \times N_t}$$

are orthogonal matrices. Then $\mathbb{V}_R^{(\mathrm{rb})}$ in (4.4) is the matrix containing the first R columns of $\mathbb{W}$, under the assumption that the singular values in Σ are sorted in decreasing order.

Next, we define

$$\varphi_i^{(\mathrm{rb})} = \sum_{j=1}^{N} (\boldsymbol{w}_i)_j \varphi_j \quad \text{and} \quad V_R^{(\mathrm{rb})} = \operatorname{span}\Big\{\varphi_1^{(\mathrm{rb})}, \dots, \varphi_R^{(\mathrm{rb})}\Big\}.$$

The Galerkin discretization of (4.1) in the reduced space $V_R^{(\mathrm{rb})} \subset V_N$ reads: For each $\boldsymbol{y} \in \mathrm{U}$, find $u_R^{(\mathrm{rb})}(\boldsymbol{y}) \in V_R^{(\mathrm{rb})}$ such that

$$\mathsf{a}\Big(u_R^{(\mathrm{rb})}(\boldsymbol{y}), v_R^{(\mathrm{rb})}; \boldsymbol{y}\Big) = \mathsf{g}\Big(v_R^{(\mathrm{rb})}; \boldsymbol{y}\Big), \quad \forall v_R^{(\mathrm{rb})} \in V_R^{(\mathrm{rb})},$$

which in algebraic form reads

$$\mathbb{A}_R^{(\mathrm{rb})}(\boldsymbol{y}) \boldsymbol{a}_R^{(\mathrm{rb})}(\boldsymbol{y}) = \boldsymbol{g}_R^{(\mathrm{rb})}(\boldsymbol{y}),$$

where

$$\Big(\mathbb{A}_R^{(\mathrm{rb})}(\boldsymbol{y})\Big)_{\ell,m} = \mathsf{a}\Big(\varphi_m^{(\mathrm{rb})}, \varphi_\ell^{(\mathrm{rb})}; \boldsymbol{y}\Big) \quad \text{and} \quad \Big(\boldsymbol{g}_R^{(\mathrm{rb})}(\boldsymbol{y})\Big)_\ell = \mathsf{g}\Big(\varphi_\ell^{(\mathrm{rb})}; \boldsymbol{y}\Big), \quad \ell, m = 1, \dots, R,$$

or equivalently

$$\mathbb{A}_R^{(\mathrm{rb})}(\boldsymbol{y}) = \mathbb{V}_R^{(\mathrm{rb})\dagger} \mathbb{A}_N(\boldsymbol{y}) \mathbb{V}_R^{(\mathrm{rb})} \in \mathbb{C}^{R \times R} \quad \text{and} \quad \boldsymbol{g}_R^{(\mathrm{rb})}(\boldsymbol{y}) = \mathbb{V}_R^{(\mathrm{rb})\dagger} \boldsymbol{g}_N(\boldsymbol{y}). \tag{4.5}$$

Remark 4.1 (Criterium to select R)**.** Provided a target tolerance $\epsilon_{\mathrm{svd}} > 0$, we select R as the smallest integer such that it holds

$$\frac{\sum_{n=1}^{R} \sigma_n^2}{\sum_{n=1}^{r} \sigma_n^2} > 1 - \epsilon_{\mathrm{svd}}^2,$$

where $\sigma_1 \geq \cdots \geq \sigma_r > 0$ are the singular values of $\mathbb{S}$, with $r = \operatorname{rank}(\mathbb{S})$.

4.2. Reduced basis construction

We now present how effectively apply the Galerkin POD method discussed in Section 4.1 in the construction of a reduced basis for the multiple arc problem.

Initially, one can attempt to directly apply the method to the entire problem. However, its performance in addressing the multiple arc problem is significantly hindered by two primary factors:

(1) To construct the snapshot matrix, a significant number of parametric configurations with multiple arcs would be necessary. Each configuration is computationally demanding, especially as the number of arcs increases
(2) The solution manifold (and its discrete counterpart) becomes difficult to approximate as it accounts for shape variations of each crack.

Even for a moderate number of arcs, a direct application of the Galerkin-POD methods is prohibitively expensive. Following [23], we firstly construct a reduced basis using the Galerkin-POD method for a single arc. Then, in the online stage, this basis is used as reduced order model for each individual arc.

4.2.1. Reduced basis construction for a single arc

Using the notation of Section 2.3, we define a new family of parametrized open arcs as follows

$$\boldsymbol{p}(\boldsymbol{y},t) = 2B\begin{pmatrix} y_1 \\ y_2 \end{pmatrix} + \varrho(y_3)\begin{pmatrix} \cos\varphi(y_4) \\ \sin\varphi(y_4) \end{pmatrix} t + \sum_{n\geq 1} y_{n+4}\boldsymbol{r}_n(t), \quad t\in[-1,1], \quad \boldsymbol{y}\in \mathrm{U},$$

where

$$\varrho(z) = (r_{\max}-r_{\min})(z+\frac{1}{2}) + r_{\min}, \quad \varphi(z) = \pi\left(z+\frac{1}{2}\right). \tag{4.6}$$

We also define the corresponding set of all possible geometries and its dimension-truncated counterpart as

$$\Sigma = \{\boldsymbol{p}(\boldsymbol{y},\cdot):\ \boldsymbol{y}\in \mathrm{U}\} \quad \text{and} \quad \Sigma^{(s)} = \left\{\boldsymbol{p}(\boldsymbol{y},\cdot):\ \boldsymbol{y}\in \mathrm{U}^{(s)}\right\}, \tag{4.7}$$

where as in the previous section we set $\mathrm{U}^{(s)} = \left[-\frac{1}{2},\frac{1}{2}\right]^s$.

The construction of the reduced basis follows as in Section 4.1, we consider the variational form of (3.2) for a single arc ($M=1$) parametrized by $\boldsymbol{p}(\boldsymbol{y})$. Additionally, and for reasons to be addressed ahead in Section 5.2.2, we also considered (3.2) for a rotated plane-wave, thus yielding the following problem. For each $\boldsymbol{y}\in \mathrm{U}$, we seek $\boldsymbol{u}(\boldsymbol{y}), \widetilde{\boldsymbol{u}}(\boldsymbol{y}) \in \mathbb{T}^{-\frac{1}{2}}$ such that

$$\begin{aligned}
\langle \mathbf{V}_{\boldsymbol{p}(\boldsymbol{y}),\boldsymbol{p}(\boldsymbol{y})}\boldsymbol{u}(\boldsymbol{y}), \boldsymbol{v}\rangle &= \langle \boldsymbol{e}_{(\theta)} g_{\theta,\kappa_{\mathrm{p}}}\circ \boldsymbol{p}(\boldsymbol{y}), \boldsymbol{v}\rangle, \qquad \forall \boldsymbol{v}\in \mathbb{T}^{-\frac{1}{2}},\\
\langle \mathbf{V}_{\boldsymbol{p}(\boldsymbol{y}),\boldsymbol{p}(\boldsymbol{y})}\widetilde{\boldsymbol{u}}(\boldsymbol{y}), \boldsymbol{v}\rangle &= \langle \boldsymbol{e}_{(\theta+\frac{\pi}{2})} g_{\theta,\kappa_{\mathrm{p}}}\circ \boldsymbol{p}(\boldsymbol{y}), \boldsymbol{v}\rangle, \quad \forall \boldsymbol{v}\in \mathbb{T}^{-\frac{1}{2}},
\end{aligned}$$

and its corresponding Galerkin discretizations using the method described in Section 3.2. *i.e.* given $N\in\mathbb{N}$, for each $\boldsymbol{y}\in \mathrm{U}^{(s)}$ we seek $\boldsymbol{u}_N(\boldsymbol{y}), \widetilde{\boldsymbol{u}}_N(\boldsymbol{y}) \in \mathbb{T}_N$ such that

$$\left\langle \mathbf{V}_{\boldsymbol{p}(\boldsymbol{y}),\boldsymbol{p}(\boldsymbol{y})}\boldsymbol{u}_N(\boldsymbol{y}), \boldsymbol{v}_N\right\rangle = \left\langle \boldsymbol{e}_{(\theta)} g_{\theta,\kappa_{\mathrm{p}}}\circ \boldsymbol{p}(\boldsymbol{y}), \boldsymbol{v}_N\right\rangle, \qquad \forall \boldsymbol{v}_N\in \mathbb{T}_N, \tag{4.8}$$

$$\left\langle \mathbf{V}_{\boldsymbol{p}(\boldsymbol{y}),\boldsymbol{p}(\boldsymbol{y})}\widetilde{\boldsymbol{u}}_N(\boldsymbol{y}), \boldsymbol{v}_N\right\rangle = \left\langle \boldsymbol{e}_{(\theta+\frac{\pi}{2})} g_{\theta,\kappa_{\mathrm{p}}}\circ \boldsymbol{p}(\boldsymbol{y}), \boldsymbol{v}_N\right\rangle, \quad \forall \boldsymbol{v}_N\in \mathbb{T}_N. \tag{4.9}$$

For a given, fixed incident angle θ, we consider the solution manifolds

$$\mathcal{M}^{\theta} \coloneqq \left\{\boldsymbol{u}(\boldsymbol{y})\in \mathbb{T}^{-\frac{1}{2}}:\ \boldsymbol{y}\in \mathrm{U}\right\}, \quad \mathcal{M}^{\theta+\frac{\pi}{2}} \coloneqq \left\{\widetilde{\boldsymbol{u}}(\boldsymbol{y})\in \mathbb{T}^{-\frac{1}{2}}:\ \boldsymbol{y}\in \mathrm{U}\right\}$$

and its discrete counterparts

$$\mathcal{M}_N^{\theta} \coloneqq \{\boldsymbol{u}_N(\boldsymbol{y})\in \mathbb{T}_N:\ \boldsymbol{y}\in \mathrm{U}\}, \quad \mathcal{M}_N^{\theta+\frac{\pi}{2}} \coloneqq \{\widetilde{\boldsymbol{u}}_N(\boldsymbol{y})\in \mathbb{T}_N:\ \boldsymbol{y}\in \mathrm{U}\}.$$

For the approximation of the discrete solution manifolds $\mathcal{M}_N^{\theta}$ and $\mathcal{M}_N^{\theta+\frac{\pi}{2}}$, we construct a snapshot matrix by sampling both problems in the parameter space. We then obtain a reduced space denoted by $V_R^{(\mathrm{rb})}$, with $R<4(N+1)$.

4.2.2. Reduced basis for the multiple arc problem

Let $V_R^{(\mathrm{rb})} = \operatorname{span}\{\boldsymbol{\varphi}_{\boldsymbol{1}}^{(\mathrm{rb})},\dots,\boldsymbol{\varphi}_{\boldsymbol{R}}^{(\mathrm{rb})}\}$ be the reduced space of the single arc problem, constructed as in Section 4.2.1. Then, for $\boldsymbol{y}^1,\dots,\boldsymbol{y}^M\in \mathrm{U}$, the Galerkin problem in the reduced basis reads as follows.

Problem 4.2. We seek $\boldsymbol{a}_R^{(\mathrm{rb}),1}(\boldsymbol{y}^1,\dots,\boldsymbol{y}^M),\dots,\boldsymbol{a}_R^{(\mathrm{rb}),M}(\boldsymbol{y}^1,\dots,\boldsymbol{y}^M)\in\mathbb{C}^R$, such that

$$\sum_{j=1}^{M} \mathbb{A}_R^{(\mathrm{rb})}\left(\boldsymbol{y}^1,\dots,\boldsymbol{y}^M\right)_{k,j}\boldsymbol{a}_R^{(\mathrm{rb}),j}\left(\boldsymbol{y}^1,\dots,\boldsymbol{y}^M\right) = \boldsymbol{g}_{R,k}^{(\mathrm{rb})}, \quad k\in\{1,\dots,M\},$$

where

$$\left(\mathbb{A}_R^{(\mathrm{rb})}(\boldsymbol{y}^1,\ldots,\boldsymbol{y}^M)_{k,j}\right)_{\ell,m} = \left\langle \boldsymbol{V}_{\boldsymbol{r}^k(\boldsymbol{y}^k),\boldsymbol{r}^j(\boldsymbol{y}^j)}\boldsymbol{\varphi}_m^{(\mathrm{rb})}, \boldsymbol{\varphi}_\ell^{(\mathrm{rb})}\right\rangle, \quad \ell,m \in \{1,\ldots,R\},$$

and

$$\left(\boldsymbol{g}_{R,k}^{(\mathrm{rb})}\right)_\ell = \left\langle \boldsymbol{g}_k, \boldsymbol{\varphi}_\ell^{(\mathrm{rb})}\right\rangle, \quad \ell \in \{1,\ldots,R\}.$$

The reduced basis approximation of the unknown $\boldsymbol{u}^{(\mathrm{rb}),j}(\boldsymbol{y}^1,\ldots\boldsymbol{y}^M)$ of (3.2), for $j=1,\ldots,M$, is then given by

$$\boldsymbol{u}^{(\mathrm{rb}),j}(\boldsymbol{y}^1,\ldots\boldsymbol{y}^M) = \sum_{l=1}^{R}(\boldsymbol{a}_R^{(\mathrm{rb}),j}(\boldsymbol{y}_1,\ldots,\boldsymbol{y}_M))_l\boldsymbol{\varphi}_l^{(\mathrm{rb})}.$$

4.3. Reduced basis linear system construction

The newly constructed linear system, which stems from the projection of the linear system of equations arising from the high-fidelity model, is of substancial smaller size than that of the high-fidelity one. However, to fully benefit from the reduced order basis method one needs to be able to efficiently compute the full-order linear system of equations in the online phase of the RB method. In particular if the approach of (4.5) is used, the cost of the assembling the linear system for the high-fidelity model (see Sect. 3.2) it would neglect any benefit of the reduced basis.

A common solution to improve the performance of the construction of the linear system, in the context where many evaluations for different parameters are required, is the Empirical Interpolation Method (EIM), see Chapter 5 from [29]. In what follows we briefly introduce the latter method and explain how is used for the multiple arc problem.

Given a function $f:(t,\boldsymbol{y})\mapsto f(t,\boldsymbol{y})$, where t is called the physical variable, and $\boldsymbol{y}\in[-1,1]^{\mathbb{N}}$ are the parameters representing the perturbations, the idea of the EIM is to construct an approximation of f of the form:

$$f(t_j,\boldsymbol{y}) \approx \sum_{q=1}^{Q} c_q(\boldsymbol{y})f(t_j,\boldsymbol{y}_q), \quad j=1,\ldots,N_c$$

where t_j, $j=1,\ldots,N_c$ represent a set of pre-fixed points. The construction of this approximation is done in two stages.

(i) **Offline Stage.** Given a discretization of U, we find $Q\in\mathbb{N}$, select the points $\boldsymbol{y}_q$, $q=1,\ldots Q$ of the discretization of U, construct the functions $c_q(\cdot)$, $q=1,\ldots,Q$ and store the values $f(t_j,\boldsymbol{y}_q)$ for future evaluations. These quantities are found using a greedy algorithm, in which is necessary to evaluate $f(t_j,\boldsymbol{z})$ for all the possible values of t_j, and $\boldsymbol{z}$ in the discretization of U. While this can be very expensive, since the processes is independent of $\boldsymbol{y}$ (the parameter for which we want to evaluate the approximation), it has to be done only one time.

(ii) **Online Stage.** Given $\boldsymbol{y}\in$ U we evaluate the functions $c_q(\boldsymbol{y})$, $q=1,\ldots,Q$ and the corresponding of approximations of $f(t_j,\boldsymbol{y})$.

Practical algorithms for the multiple arcs cases are given in the next section.

4.3.1. EIM for multiples open arcs

We now explain how to use the EIM for the construction of the reduced linear system for the multiple arcs problem.

To solve the multiple arcs problem in the reduced basis space one needs to assemble the linear system of equations described in Problem 4.2. This implies the computation of M^2 block matrices: M blocks accounting for self-interaction terms, and M^2-M for cross interaction between arcs. It follows from (4.5) that each of these blocks are of the form

$$\mathbb{A}_R^{(\mathrm{rb})}(\boldsymbol{y}^1,\ldots,\boldsymbol{y}^M)_{k,j} = \mathbb{V}_R^{(\mathrm{rb})\dagger}\mathbb{A}_N(\boldsymbol{y}^1,\ldots,\boldsymbol{y}^M)_{k,j}\mathbb{V}_R^{(\mathrm{rb})}, \tag{4.10}$$

where $\mathbb{A}_N(\boldsymbol{y}^1,\dots,\boldsymbol{y}^M)_{k,j}$ corresponds to the matrix accounting for the interaction between arcs k,j in the high-fidelity space[4]. Furthermore, notice that while the full matrices $\mathbb{A}_R^{(\mathrm{rb})}(\boldsymbol{y}^1,\dots,\boldsymbol{y}^M)$, and $\mathbb{A}_N(\boldsymbol{y}^1,\dots,\boldsymbol{y}^M)$ depends on M parameters, the block k,j only depends on $\boldsymbol{y}^k$ and $\boldsymbol{y}^j$. In the following, we simplify the notation but just including the two active parameters as arguments.

Let us consider first the computation of $(\mathbb{A}_R^{(\mathrm{rb})}(\boldsymbol{y}^k,\boldsymbol{y}^j))_{k,j}$, for $k\neq j$. The the case $k=j$ is treated at the end of this section. According to Remark 3.4 and (4.10), there exists a linear function L, such that

$$\mathbb{A}_N(\boldsymbol{y}^k,\boldsymbol{y}^j)_{k,j}\approx L\big(\mathfrak{G}_{k,j}(\boldsymbol{y}^k,\boldsymbol{y}^j)\big),$$

where $\mathfrak{G}_{k,j}(\boldsymbol{y}_1,\boldsymbol{y}_2)$, is a matrix constructed from evaluations of the fundamental solution, *i.e.* consider N_c points $\{x_p\}_{p=1}^{N_c}\subset(-1,1)$

$$\mathfrak{G}_{k,j}(\boldsymbol{y}^k,\boldsymbol{y}^j)=\begin{pmatrix}\mathbf{G}(\boldsymbol{r}^k(\boldsymbol{y}^k)(x_1),\boldsymbol{r}^j(\boldsymbol{y}^j)(x_1)) & \cdots & \mathbf{G}(\boldsymbol{r}^k(\boldsymbol{y}^k)(x_1),\boldsymbol{r}^j(\boldsymbol{y}^j)(x_{N_c}))\\ \vdots & \ddots & \vdots\\ \mathbf{G}(\boldsymbol{r}^k(\boldsymbol{y}^k)(x_{N_c}),\boldsymbol{r}^j(\boldsymbol{y}^j)(x_1)) & \cdots & \mathbf{G}(\boldsymbol{r}^k(\boldsymbol{y}^k)(x_{N_c}),\boldsymbol{r}^j(\boldsymbol{y}^j)(x_{N_c}))\end{pmatrix}.$$

By introducing the linear function $L^R(\cdot)=(\mathbb{V}_R^{(\mathrm{rb})})^\dagger L(\cdot)\mathbb{V}_R^{(\mathrm{rb})}$, we can write an approximation of $\mathbb{A}_R^{(\mathrm{rb})}(\boldsymbol{y}^k,\boldsymbol{y}^j)_{k,j}$, as

$$\mathbb{A}_R^{(\mathrm{rb})}(\boldsymbol{y}^k,\boldsymbol{y}^j)_{k,j}\approx L^R(\mathfrak{G}_{k,j}(\boldsymbol{y}^k,\boldsymbol{y}^j)).$$

Now we would use the EIM to form an interpolation of $\mathfrak{G}_{\boldsymbol{k,j}}(\boldsymbol{y}_1,\boldsymbol{y}_2)$, this will result in an approximation of $\mathbb{A}_R^{(\mathrm{rb})}(\boldsymbol{y}^k,\boldsymbol{y}^j)_{k,j}$, once the linear map L^R is applied to the interpolated evaluations.

Without any further assumptions for each of the M^2-M off-diagonal blocks we have to compute a tailored interpolation based on the EIM for each pair of interactions. To reduce the computational burden, we instead form a global interpolation of $\mathfrak{G}_{k,j}(\boldsymbol{y}^k,\boldsymbol{y}^j)$ incorporating the local indices k,j in the interpolation variables.

To this end, given $s\in\mathbb{N}$, and $\boldsymbol{y}^k,\boldsymbol{y}^j\in\mathrm{U}^s$, we define $\boldsymbol{z}^{k,j}\in\mathrm{U}^{2s+6}$, whose components are

$$\begin{aligned}
z_1^{k,j}&=\left(\frac{\varrho_k-r_{\min}}{r_{\max}-r_{\min}}\right)-\frac{1}{2}\\
z_2^{k,j}&=\frac{\varphi_k}{\pi}-\frac{1}{2}\\
z_{n+2}^{k,j}&=(y^k)_n,\quad n=1,\dots,s\\
z_{s+3}^{k,j}&=\left(\frac{d-d_{\min}}{d_{\max}-d_{\min}}\right)-\frac{1}{2},\quad d=\|\boldsymbol{c}_k-\boldsymbol{c}_j\|\\
z_{s+4}^{k,j}&=\frac{\theta}{\pi}-\frac{1}{2},\quad \theta=\arg(\boldsymbol{c}_k-\boldsymbol{c}_j)\\
z_{s+5}^{k,j}&=\left(\frac{\varrho_j-r_{\min}}{r_{\max}-r_{\min}}\right)-\frac{1}{2}\\
z_{s+6}^{k,j}&=\frac{\varphi_j}{\pi}-\frac{1}{2}\\
z_{n+s+6}^{k,j}&=(y^j)_n,\quad n=1,\dots,s
\end{aligned}$$

where $r_{\min},r_{\max},d_{\min},d_{\max}$ are the global geometry parameters defined in Section 2.3 and $\boldsymbol{c}_j,\boldsymbol{c}_k,\varrho_j,\varrho_k,\varphi_j,\varphi_k$ are the variables determining the fixed part of arcs k,j respectively, also defined in the same section.

[4]This is the same matrix $\mathbb{A}_{k,j}$ of Section 3.2, but we have made explicit the dependence of the parameters as its makes the use of the EIM more clear.

For a general $\boldsymbol{z} \in \mathrm{U}^{2s+6}$ we introduce the following auxiliary parametrizations:

$$\boldsymbol{h}_1(\boldsymbol{z},t) = \varrho(z_1)\begin{pmatrix}\cos\varphi(z_2)\\ \sin\varphi(z_2)\end{pmatrix}t + \sum_{n=1}^{s} z_{n+2}\boldsymbol{r}_n(t), \tag{4.11a}$$

$$\boldsymbol{h}_2(\boldsymbol{z},t) = d(z_{s+3})\begin{pmatrix}\cos\varphi(z_{s+4})\\ \sin\varphi(z_{s+4})\end{pmatrix} + \varrho(z_{s+5})\begin{pmatrix}\cos\varphi(z_{s+6})\\ \sin\varphi(z_{s+6})\end{pmatrix}t + \sum_{n=1}^{s} z_{n+s+6}\boldsymbol{r}_n(t), \tag{4.11b}$$

where $d(z) = (d_{\max} - d_{\min})(z + \frac{1}{2}) + d_{\min}$, and the functions ϱ, φ are the same that in (4.6). Finally using the in-variance of the fundamental solution under translations we have that,

$$\mathbf{G}(\boldsymbol{r}^k(\boldsymbol{y}^k,t), \boldsymbol{r}^j(\boldsymbol{y}^j,\tau) = \mathbf{G}(\boldsymbol{h}_1(\boldsymbol{z}^{k,j},t), \boldsymbol{h}_2(\boldsymbol{z}^{k,j},\tau)), \quad \forall t,\tau \in [-1,1].$$

This last equation justify the fact that we only need to construct an interpolation of the function:

$$\mathbb{H}(x_p, x_q, \boldsymbol{z}) = \mathbf{G}(\boldsymbol{h}_1(\boldsymbol{z}, x_p), \boldsymbol{h}_2(\boldsymbol{z}, x_q)), \quad p,q = 1,\dots,N_c.$$

The implementation of the EIM for this particular functions is given in Algorithm 1 for the offline part, and Algorithm 2 for the online evaluation[5].

Remark 4.3. Lines 19, and 20, of Algorithm 1, ensure that the matrix $\mathfrak{I}_S$, is a triangular matrix, and then corresponding linear system, on Algorithm 2 can be solved fast. Alternatively, we could replace these two lines by their simpler counterparts,

$$\mathfrak{I}_B \leftarrow H[\ell_{\max}][:]$$
$$\mathfrak{I}_M \leftarrow L^R(H[\ell_{\max}][:])$$

and then instead of returning the square matrix $\mathfrak{I}_B[:][X_{\max}]$, we return its inverse, so the evaluation in Algorithm 2, can be carried out fast. This alternative could lead to ill-conditioned linear system in Algorithm 1, however since these are typically very small and solved by direct methods no extra complications arise. The main advantage of using this procedure is that in some implementations evaluating

$$L^R\left(\frac{H[\ell_{\max}][:] - \mathfrak{I}[\ell_{\max}][:]}{H[\ell_{\max}][x_{\max}] - \mathfrak{I}[\ell_{\max}][x_{\max}]}\right)$$

may not be supported, but $L^R(H[\ell_{\max}][:])$ is just a discretization matrix.

In terms of computational cost, since we are interested in solving for a number of geometric configurations, the only relevant part is Algorithm 2. For each cross-interaction the cost is $O(Q^2 + R^2Q)$.

Finally, let us comment in the approximation of the self-interaction matrices. As mentioned in Remark 3.4, in an abstract setting the only difference between cross and self-interactions is that for the self-interactions we have two different functions (a regular part, and the function $J(t,\tau)$ of Rem. 3.4). Thus, we need to interpolate two different functions, but in essence the costs and algorithms are the same.

With this final considerations we have that total cost of the construction of the linear system is $O(M^2(Q^2 + R^2Q))$, compared with $O(M^2N^2 \log \mathrm{N})$ for the high-fidelity solver of Section 3.2.

[5]In these algorithms we use the following notation, if A is a two-dimensional array (matrix), its element (j,k), is denoted by $A[j][k]$, its row j is $A[j][:]$, and its column k is $A[:][k]$.

Algorithm 1. Empirical Interpolation Method: Offline Phase.

procedure EIM_OFFLINE_KERNEL($\epsilon_{eim}, \boldsymbol{z}_s, Q_{\max}, QuadPoints$)
  $N_s = length(z_s)$
  for $\ell = 1, \ldots, N_s$ **do**
    $H[\ell][:] = \mathbb{H}(QuadPoints, \boldsymbol{z}_s(\ell))$ ▷ Pre-compute the evaluations $\mathbb{H}$
  end for
  $\mathfrak{I} = zeros$ ▷ Initialize interpolation for all the geometries in $\boldsymbol{z_s}$
  $e_{\max} = 1e28$ ▷ The error initialized as a big number
  $\mathfrak{I}_B = []$ ▷ Stores the interpolation basis
  $\mathfrak{I}_M = []$ ▷ Stores the interaction matrices, $L^R(\mathfrak{I}_B)$
  $X_{\max} = []$ ▷ Stores indices of the quadrature points where big errors are detected
  while $q < Q_{\max}$ and $e_{\max} > \epsilon_{eim}$ **do**
    for $\ell = 1, \ldots, N_s$ **do**
      $\text{Error}(\ell) = \frac{\|H[\ell][:] - \mathfrak{I}[\ell][:]\|}{\|H[\ell][:]\|}$
    end for
    $\ell_{\max} = \text{argmax}(\text{Error})$
    $\text{e}_{\max} = \text{Error}(\ell_{\max})$
    $\text{x}_{\max} = \text{argmax}(\frac{\|H[\ell_{\max}][:] - \mathfrak{I}[\ell_{\max}][:]\|}{\|H[\ell_{\max}][:]\|})$
    $X_{\max} \leftarrow x_{\max}$
    $\mathfrak{I}_B \leftarrow \frac{H[\ell_{\max}][:] - \mathfrak{I}[\ell_{\max}][:]}{H[\ell_{\max}][x_{\max}] - \mathfrak{I}[\ell_{\max}][x_{\max}]}$
    $\mathfrak{I}_M \leftarrow L^R\left(\frac{H[\ell_{\max}][:] - \mathfrak{I}[\ell_{\max}][:]}{H[\ell_{\max}][x_{\max}] - \mathfrak{I}[\ell_{\max}][x_{\max}]}\right)$
    $g = (H[:][X_{\max}])^\top$
    $c = \text{LinSolve}(\mathfrak{I}_B[:][X_{\max}], g)$
    $\mathfrak{I} = (\mathfrak{I}_B)c$
  end while
  $\mathfrak{I}_s = \mathfrak{I}_B[:][X_{\max}]$
  Return $\mathfrak{I}_S, \mathfrak{I}_M, X_{\max}$
end procedure

Algorithm 2. EIM Evaluation.

procedure EIM_ONLINE($QuadPoints, \boldsymbol{z}, \mathfrak{I}_S, X_{\max}, \mathfrak{I}_M$)
  $\boldsymbol{g} = \mathbb{H}(QuadPoints[X_{\max}], \boldsymbol{z})$ ▷ Evaluate the Fundamental solution for the configuration z, but only on the specified quadrature points
  $\boldsymbol{c} = \text{LinSolve}(\mathfrak{I}_S, g)$ ▷ Obtain the coefficients to exactly interpolate the configuration given by z in the specified Quadrature points
  $Interp = \mathfrak{I}_M \boldsymbol{c}$ ▷ Construction of the interpolation
  Return $Interp$
end procedure

5. Analysis of the reduced basis method for multiple open arcs

In this section, we provide an analysis of the reduced basis method for the multiple arc problem described in Section 4.

5.1. Parametric holomorphy

We establish the analytic or holomorphic dependence of the *discrete* parameter-to-solution map upon the the parametric variables used to describe the arc's shapes. This property is of key importance for the derivation of the convergence analysis presented in Section 5.2. The results to be presented herein are based on our previous work [37].

For $\rho > 1$, we consider the Bernstein ellipse in the complex plane

$$\mathcal{E}_\rho := \left\{ \frac{z + z^{-1}}{2} : 1 \leq |z| \leq \rho \right\} \subset \mathbb{C}.$$

This ellipse has foci at $z = \pm 1$ and semi-axes of length $a := \frac{1}{2}(\varrho + \varrho^{-1})$ and $b := \frac{1}{2}(\varrho - \varrho^{-1})$. Let us consider the tensorized poly-ellipse

$$\mathcal{E}_{\boldsymbol{\rho}} := \bigotimes_{j \geq 1} \mathcal{E}_{\rho_j} \subset \mathbb{C}^{\mathbb{N}},$$

where $\boldsymbol{\rho} := \{\rho_j\}_{j \geq 1}$ is such that $\rho_j > 1$, for $j \in \mathbb{N}$.

Definition 5.1 ([11], Def. 2.1)**.** Let X be a *complex* Banach space equipped with the norm $\|\cdot\|_X$. For $\varepsilon > 0$ and $p \in (0, 1)$, we say that the map

$$\mathrm{U} \ni \boldsymbol{y} \mapsto u(\boldsymbol{y}) \in X$$

is $(\boldsymbol{b}, p, \varepsilon)$-holomorphic if and only if

(i) The map $\mathrm{U} \ni \boldsymbol{y} \mapsto u(\boldsymbol{y}) \in X$ is uniformly bounded, *i.e.*

$$\sup_{\boldsymbol{y} \in \mathrm{U}} \|u(\boldsymbol{y})\|_X \leq C_0,$$

for some finite constant $C_0 > 0$.

(ii) There exists a positive sequence $\boldsymbol{b} := \{b_j\}_{j \geq 1} \in \ell^p(\mathbb{N})$ and a constant $C_\varepsilon > 0$ such that for any sequence $\boldsymbol{\rho} := \{\rho_j\}_{j \geq 1}$ of numbers strictly larger than one that is $(\boldsymbol{b}, \varepsilon)$-admissible, *i.e.* satisfying

$$\sum_{j \geq 1} (\rho_j - 1) b_j \leq \varepsilon,$$

the map $\boldsymbol{y} \mapsto u(\boldsymbol{y})$ admits a complex extension $\boldsymbol{z} \mapsto u(\boldsymbol{z})$ that is holomorphic with respect to each variable z_j on a set of the form

$$\mathcal{O}_{\boldsymbol{\rho}} := \bigotimes_{j \geq 1} \mathcal{O}_{\rho_j},$$

where $\mathcal{O}_{\rho_j} \subset \mathbb{C}$ is an open set containing $\mathcal{E}_{\rho_j}$. This extension is bounded on $\mathcal{E}_{\boldsymbol{\rho}}$ according to

$$\sup_{\boldsymbol{z} \in \mathcal{E}_{\boldsymbol{\rho}}} \|u(\boldsymbol{z})\|_X \leq C_\varepsilon.$$

By considering the parametric family of open arcs $\boldsymbol{r}(\boldsymbol{y}, \cdot) : (-1, 1) \to \mathbb{R}^2$, we define the discrete parameter-to-solution map as $\boldsymbol{y} \mapsto \boldsymbol{u}_N(\boldsymbol{y})$, where, for each $\boldsymbol{y} \in \mathrm{U}$, $\boldsymbol{u}_N(\boldsymbol{y}) \in \mathbb{T}_N$ corresponds to the solution of (4.8) on the parametrically defined open arc $\boldsymbol{r}(\boldsymbol{y})$, for a given incidence angle θ.

Lemma 5.2. *Let $m \in \mathbb{N}$ and $\alpha \in [0, 1]$ be such that $m + \alpha > 2$. Let Assumption 2.1 be satisfied with $\boldsymbol{b} \in \ell^p(\mathbb{N})$ and $p \in (0, 1)$. Then there exist $\varepsilon > 0$ and $N_0 \in \mathbb{N}$ such that for any $N \geq N_0$ the maps*

$$\mathrm{U} \ni \boldsymbol{y} \mapsto \boldsymbol{u}_N(\boldsymbol{y}), \widetilde{\boldsymbol{u}}_N(\boldsymbol{y}) \in \mathbb{T}_N$$

are $(\boldsymbol{b}, p, \varepsilon)$-holomorphic and continuous with the same $\boldsymbol{b} \in \ell^p(\mathbb{N})$ and $p \in (0, 1)$, and with $\varepsilon > 0$ independent of N, where $\boldsymbol{u}_N(\boldsymbol{y}), \widetilde{\boldsymbol{u}}_N(\boldsymbol{y})$ are the solutions of (4.8) and (4.9), respectively.

Proof. Using the projection on $\mathbb{T}_N$, and denoting the arc parametrization by $\boldsymbol{r}(\boldsymbol{y})$, we can rewrite (4.8), (4.9) as: find $\boldsymbol{u}_N(\boldsymbol{y}), \widetilde{\boldsymbol{u}}_N(\boldsymbol{y}) \in \mathbb{T}_N$ such that

$$P_{\mathbb{W}_N}\mathbf{V}_{\boldsymbol{r}(\boldsymbol{y}),\boldsymbol{r}(\boldsymbol{y})}\boldsymbol{u}_N(\boldsymbol{y}) = P_{\mathbb{W}_N}\boldsymbol{e}_{(\theta)}g_{\theta,\kappa_{\mathsf{p}}}\circ\boldsymbol{r}(\boldsymbol{y}),$$
$$P_{\mathbb{W}_N}\mathbf{V}_{\boldsymbol{r}(\boldsymbol{y}),\boldsymbol{r}(\boldsymbol{y})}\widetilde{\boldsymbol{u}}_N(\boldsymbol{y}) = P_{\mathbb{W}_N}\boldsymbol{e}_{(\theta+\frac{\pi}{2})}g_{\theta,\kappa_{\mathsf{p}}}\circ\boldsymbol{r}(\boldsymbol{y}).$$

It follows from [37] that the map $\mathrm{U} \ni \boldsymbol{y} \mapsto \mathbf{V}_{\boldsymbol{r}(\boldsymbol{y}),\boldsymbol{r}(\boldsymbol{y})}$ is $(\boldsymbol{b}, p, \epsilon)$-holomorphic and continuous for some $\epsilon > 0$.

On the other hand, $P_{\mathbb{W}_N}$ is a linear operator independent of the parameter $\boldsymbol{y}$, and $g_{\theta,\kappa_{\mathsf{p}}}\circ\boldsymbol{r}(\boldsymbol{y})$ is an entire function of the arc parametrization $\boldsymbol{r}$. Consequently, the maps

$$\mathrm{U} \ni \boldsymbol{y} \mapsto P_{\mathbb{W}_N}\mathbf{V}_{\boldsymbol{r}(\boldsymbol{y}),\boldsymbol{r}(\boldsymbol{y})} \in \mathcal{L}(\mathbb{T}_N, \mathbb{W}_N),$$

and

$$\mathrm{U} \ni \boldsymbol{y} \mapsto P_{\mathbb{W}_N}\boldsymbol{e}_{(\theta)}g_{\theta,\kappa_{\mathsf{p}}}\circ\boldsymbol{r}(\boldsymbol{y}), P_{\mathbb{W}_N}\boldsymbol{e}_{\theta+\frac{\pi}{2}}g_{\theta,\kappa_{\mathsf{p}}}\circ\boldsymbol{r}(\boldsymbol{y}) \in \mathbb{W}_N,$$

are $(\boldsymbol{b}, p, \epsilon')$-holomorphic and continuous, with ϵ independent of N.

Using the standard stability of the Galerkin discretization of an injective Fredholm operator of index 0, we can ensure that for each $\boldsymbol{y} \in \mathrm{U}$ there exist $N_0(\boldsymbol{y})$ such that $P_{\mathbb{W}_N}\mathbf{V}_{\boldsymbol{r}(\boldsymbol{y}),\boldsymbol{r}(\boldsymbol{y})}$ has a bounded inverse in $\mathcal{L}(\mathbb{T}_N, \mathbb{W}_N)$ for every $N > N_0(\boldsymbol{y})$. Next, we form an open cover of U with the sets of the form

$$A_{N_0,C} = \left\{\boldsymbol{y} \in \mathrm{U} \ : \left\|\left(P_{\mathbb{W}_N}\mathbf{V}_{\boldsymbol{r}(\boldsymbol{y}),\boldsymbol{r}(\boldsymbol{y})}\right)^{-1}\right\|_{\mathcal{L}(\mathbb{T}_N,\mathbb{W}_N)} < C, \text{ for } N > N_0\right\}.$$

Since U is compact we can find N_0 independent of $\boldsymbol{y}$, and then the results follows from the holomorphic extension of the inverse operation and Theorem 4.4 from [37], with a possibly different ϵ but still not depending on $N \in \mathbb{N}$. □

An equivalent statement for the multiple problem can be proved, *i.e.* parametric holomorphy of the discrete domain-to-solution map. However, as the ensuing analysis of the ROM algorithm is based on the understanding of the single arc problem, we skip it.

A commonly used concept in nonlinear approximation to quantify uniform error bounds is the so-called Kolmogorov's width. For a compact subset $\mathcal{K}$ of a Banach space X it is defined for $R \in \mathbb{N}$ as

$$d_R(\mathcal{K}, X) := \inf_{\dim(X_R)\leq R}\sup_{v\in\mathcal{K}}\inf_{w\in X_R}\|v - w\|_X,$$

where the outer infimum is taken over all finite dimensional spaces $X_R \subset X$ of dimension smaller than R. This quantifies the suitability of R-dimensional subspaces for the approximation of the solution manifold.

In particular, if we consider the response surface associated to the discrete single arc parametric problem, *i.e.* $\mathcal{M}_N^\theta$, we have as a consequence of [13] and Lemma 5.2 the following bound: there exist $N_0 \in \mathbb{N}$ such that for any $N \geq N_0$

$$d_R\left(\mathcal{M}_N^\theta, \mathbb{T}^{-\frac{1}{2}}\right) \leq CR^{-\left(\frac{1}{p}-1\right)}, \quad R \in \mathbb{N},$$

for some $C > 0$ depending only on N_0 and $p \in (0, 1)$ as in Assumption 2.1. The exact same result holds valid for the solution manifold $\mathcal{M}_N^{\theta+\frac{\pi}{2}}$.

5.2. Convergence analysis

In this section we provide a complete error analysis of the reduced basis method for multiple open arcs. The results of this section justify the algorithms from Section 4, which in turn lead to the numerical results presented ahead in Section 6.

Let $V_R^{(\mathrm{rb})}$ be as in (4.2) for $R \in \mathbb{N}$. Herein, we interested in quantifying the performance of the RB algorithm according to the following error measure

$$\varepsilon\Big(V_R^{(\mathrm{rb})}\Big) = \int_{\mathrm{U}} \cdots \int_{\mathrm{U}} \Big\| \mathfrak{u}(\boldsymbol{y}^1, \ldots, \boldsymbol{y}^M) - \mathfrak{u}_R^{(\mathrm{rb})}\Big(\boldsymbol{y}^1_{\{1:s\}}, \ldots \boldsymbol{y}^M_{\{1:s\}}\Big)\Big\|^2_{\mathbb{T}^{-\frac{1}{2}} \times \cdots \times \mathbb{T}^{-\frac{1}{2}}} \, \mathrm{d}\boldsymbol{y}^1 \cdots \mathrm{d}\boldsymbol{y}^M, \tag{5.1}$$

where $\boldsymbol{y}^1, \ldots, \boldsymbol{y}^M \in \mathrm{U}$, and $\boldsymbol{y}^j_{\{1:s\}} = (y^j_1, y^j_2, \ldots y^j_s, 0, 0 \ldots) \in \mathrm{U}$, $j = 1, \ldots, M$.

$$\mathfrak{u}(\boldsymbol{y}^1, \ldots, \boldsymbol{y}^M) = \begin{pmatrix} \boldsymbol{u}^1(\boldsymbol{y}^1, \ldots, \boldsymbol{y}^M) \\ \vdots \\ \boldsymbol{u}^M(\boldsymbol{y}^1, \ldots, \boldsymbol{y}^M) \end{pmatrix} \in \mathbb{T}^{-\frac{1}{2}} \times \cdots \times \mathbb{T}^{-\frac{1}{2}}$$

corresponds to the solution of the multiple open arcs problem. Equivalently, $\mathfrak{u}_R^{(\mathrm{rb})}(\boldsymbol{y}^1_{\{1:s\}}, \ldots \boldsymbol{y}^M_{\{1:s\}})$ is defined as the solution of reduced multiple arc problem.

In the remainder of this section we investigate appropriate bounds for $\varepsilon(V_R^{(\mathrm{rb})})$ in two cases.

(i) Firstly, in Section 5.2.1 we consider the single arc problem. The convergence analysis follows for standard arguments, as the ones presented in [29,39]. A key element in our analysis consists in bounding Kolmogorov's width of the solution manifold, which as discussed in [13], follows from the parametric holomorphy property of the parameter-to-solution map.

(ii) Secondly, in Section 5.2.2 we consider the multiple open arcs problem. The main difficulty is that the reduced basis in this case by construction are only guaranteed to provide good performance for the single arc problem. We prove that the multi-arc problem can be cast as independent single arc problems but on different geometries.

5.2.1. Convergence analysis of the single arc problem

To simplify the exposition of the multiple arcs case we enumerate the different steps needed to bound $\varepsilon(V_R^{(\mathrm{rb})})$ for the single arc problem with $V_R^{(\mathrm{rb})}$ as in Section 4.2.1.

(i) **Dimension Truncation in the Parameter Space.** As a consequence of the parametric holomorphy property of the parameter-to-solution map, and following the arguments of [20], we truncate the parametric dimension as follows

$$\varepsilon\Big(V_R^{(\mathrm{rb})}\Big) \leq \int_{\mathrm{U}^s} \Big\| \boldsymbol{u}\big(\boldsymbol{y}_{\{1:s\}}\big) - \boldsymbol{u}_R^{(\mathrm{rb})}\big(\boldsymbol{y}_{\{1:s\}}\big)\Big\|^2_{\mathbb{T}^{-\frac{1}{2}}} \, \mathrm{d}\boldsymbol{y} + C_1(p) s^{-2\left(\frac{1}{p}-1\right)},$$

for some constant $C_1(p)$ depending on $p \in (0,1)$, however not on the parametric dimension $s \in \mathbb{N}$.

(ii) **Galerkin BEM Discretization.** Recalling the convergence results established in Section 3.2, we can replace $\boldsymbol{u}(\boldsymbol{y})$ by its Galerkin approximation. Provided that the arc is analytic, as stated in Section 3.2, Remark 3.2, one has exponential convergence towards the exact solution, *i.e.* there exist $N_0 \in \mathbb{N}$, $\varrho > 1$ and $C_2 > 0$ such that for any $N \geq N_0$

$$\begin{aligned} \varepsilon\Big(V_R^{(\mathrm{rb})}\Big) \leq \int_{\mathrm{U}^s} \Big\| \boldsymbol{u}_N\big(\boldsymbol{y}_{\{1:s\}}\big) - \boldsymbol{u}_R^{(\mathrm{rb})}\big(\boldsymbol{y}_{\{1:s\}}\big)\Big\|^2_{\mathbb{T}^{-\frac{1}{2}}} \, \mathrm{d}\boldsymbol{y} \\ + C_2 \varrho^{-2N} + C_1(p) s^{-2\left(\frac{1}{p}-1\right)}. \end{aligned}$$

(iii) **Quasi-optimality in the Reduced Space.** Since $\boldsymbol{u}_R^{(\mathrm{rb})}$ is obtained by solving a Galerkin discretization of a well-posed and coercive problem, quasi-optimality yields the existence of a unique discrete solution for

R large enough. *i.e.*, there exists $R_0 > 0$ and $C_3 > 0$, such that for any $R \geq R_0$ one has

$$\varepsilon\Big(V_R^{(\mathrm{rb})}\Big) \leq C_3 \int_{\mathrm{U}^s} \Big\| \boldsymbol{u}_N\big(\boldsymbol{y}_{\{1:s\}}\big) - P_R^{(\mathrm{rb})} \boldsymbol{u}_N\big(\boldsymbol{y}_{\{1:s\}}\big) \Big\|^2_{\mathbb{T}^{-\frac{1}{2}}} \,\mathrm{d}\boldsymbol{y} + C_2 \varrho^{-2N} + C_1(p) s^{-2\left(\frac{1}{p}-1\right)},$$

where $P_R^{(\mathrm{rb})} : \mathbb{T}_N \to V_R^{(\mathrm{rb})}$ denotes the orthogonal projection operator onto the reduced space $V_R^{(\mathrm{rb})}$, and C_3 depends only on R_0.

(iv) **Decay of the Kolmmogorov's Width.** As a consequence of Lemma 5.2, which in turn follows from our previous work [37] and the stability of the Galerkin BEM discetrization described in Section 3.2, and [13] we may conclude that there exists $C_4 > 0$ such that for $R \geq R_0$ and $N \geq N_0$, with R_0 as in item (iii) and N_0 as in item (ii), we have

$$\varepsilon\Big(V_R^{(\mathrm{rb})}\Big) \leq C_4 R^{-2\left(\frac{1}{p}-1\right)} + C_2 \varrho^{-2N} + C_1(p) s^{-2\left(\frac{1}{p}-1\right)}.$$

Clearly, the computation of $V_R^{(\mathrm{rb})}$ is not feasible as it requires the evaluation of (4.2). Therefore, we consider a discrete approximation of the high-dimensional integral as in (4.4), and we refer to this space as $\widetilde{V}_R^{(\mathrm{rb})}$. To quantify this mismatch, we follow ([39], Sect. 6.5).

Set

$$\varepsilon^{(N_s)}\Big(\widetilde{V}_R^{(\mathrm{rb})}\Big) = \frac{1}{N_t} \sum_{j=1}^{N_t} \Big\| \boldsymbol{u}_N(\boldsymbol{y}_j) - P_R^{(\mathrm{rb})} \boldsymbol{u}_N(\boldsymbol{y}_j) \Big\|^2_{\mathbb{T}^{-\frac{1}{2}}}.$$

We are interested in the performance of this empirically constructed space according to

$$\varepsilon\Big(\widetilde{V}_R^{(\mathrm{rb})}\Big) \leq \underbrace{\Big|\varepsilon\Big(\widetilde{V}_R^{(\mathrm{rb})}\Big) - \varepsilon^{(N_s)}\Big(\widetilde{V}_R^{(\mathrm{rb})}\Big)\Big|}_{(\clubsuit)} + \varepsilon^{(N_s)}\Big(\widetilde{V}_R^{(\mathrm{rb})}\Big).$$

It follows from [24] that for each $\delta > 0$ there exists $C(\delta) > 0$ such that $(\clubsuit) \leq C(\delta) N^{-1+\delta}$, and with $C(\delta) \to \infty$ as $\delta \to 0^+$. The last term can be bounded by the singular values of the snapshot matrix.

5.2.2. Convergence analysis for multiple open arcs

We proceed to establish the convergence of the RB method applied to the multiple arcs problem as described in Section 4.2.2. Throughout, we work under the following assumption.

Assumption 5.3. *The set Σ defined in (4.7) is closed under rotations, i.e. if $\boldsymbol{r} \in \Sigma$, then for any $\theta \in [0, 2\pi)$, $\boldsymbol{R}_\theta \boldsymbol{r} \in \Sigma$, where $\boldsymbol{R}_\theta$ denotes the rotation matrix for angle θ defined in (2.1). In addition, for $s \in \mathbb{N}$, $s > 4$, the set Σ_s is closed under rotations as well.*

Remark 5.4. (i) For $s = 4$ is immediate that Σ_s is closed under rotations as they are only line segments in $\mathbb{R}^2$.

(ii) For larger values of s, *i.e.* $s > 4$, in general it would depend on the properties of the functions $\{\boldsymbol{r}_n\}_{n\in\mathbb{N}}$.

(iii) A particular case for which one may straightforwardly verify Assumption 5.3 is when the functions $\{\boldsymbol{r}_n\}_{n\in\mathbb{N}}$ are of the form $r_n \boldsymbol{e}_1$, $r_n \boldsymbol{e}_2$, for some scalar functions r_n, and for each $n \in \mathbb{N}$.

For the sake of simplicity, we firstly discuss the two open arcs problem as the extension to multiple open arcs follows from the exact same arguments. This problem reads as follows: For $\boldsymbol{y}^1, \boldsymbol{y}^2 \in \mathrm{U}$, we seek $\boldsymbol{u}^1(\boldsymbol{y}^1, \boldsymbol{y}^2), \boldsymbol{u}^2(\boldsymbol{y}^1, \boldsymbol{y}^2) \in \mathbb{T}^{-\frac{1}{2}}$ such that

$$\begin{aligned} \boldsymbol{V}_{\boldsymbol{r}^1(\boldsymbol{y}^1),\boldsymbol{r}^1(\boldsymbol{y}^1)} \boldsymbol{u}^1(\boldsymbol{y}^1, \boldsymbol{y}^2) + \boldsymbol{V}_{\boldsymbol{r}^1(\boldsymbol{y}^1),\boldsymbol{r}^2(\boldsymbol{y}^2)} \boldsymbol{u}^2(\boldsymbol{y}^1, \boldsymbol{y}^2) &= \boldsymbol{g}_1, \\ \boldsymbol{V}_{\boldsymbol{r}^2(\boldsymbol{y}^2),\boldsymbol{r}^1(\boldsymbol{y}^1)} \boldsymbol{u}^1(\boldsymbol{y}^1, \boldsymbol{y}^2) + \boldsymbol{V}_{\boldsymbol{r}^2(\boldsymbol{y}^2),\boldsymbol{r}^2(\boldsymbol{y}^2)} \boldsymbol{u}^2(\boldsymbol{y}^1, \boldsymbol{y}^2) &= \boldsymbol{g}_2, \end{aligned}$$

where $\boldsymbol{g}_1, \boldsymbol{g}_2$ are as in (3.3).

The analysis of the multiple arc problem has one major difference compered to the single arc case: In the former case the cross-interaction terms cannot be accounted for by the use of the reduced space.

In the following we argue that the solution of the multiple open arc problem can be approximated (in a controlled way) by a linear combinations of independent problem, posed on different geometries. First notice that the multi-arc problem can be expressed as

$$\boldsymbol{V}_{\boldsymbol{r}^1(\boldsymbol{y}^1),\boldsymbol{r}^1(\boldsymbol{y}^1)}\boldsymbol{u}^1(\boldsymbol{y}^1,\boldsymbol{y}^2) = \boldsymbol{f}_1(\boldsymbol{y}^1,\boldsymbol{y}^2) \quad \text{and} \quad \boldsymbol{V}_{\boldsymbol{r}^2(\boldsymbol{y}^2),\boldsymbol{r}^2(\boldsymbol{y}^2)}\boldsymbol{u}^2(\boldsymbol{y}^1,\boldsymbol{y}^2) = \boldsymbol{f}_2(\boldsymbol{y}^1,\boldsymbol{y}^2),$$

where

$$\begin{aligned}\boldsymbol{f}_1(\boldsymbol{y}^1,\boldsymbol{y}^2) &= \boldsymbol{g}_1 - \boldsymbol{V}_{\boldsymbol{r}^1(\boldsymbol{y}^1),\boldsymbol{r}^2(\boldsymbol{y}^2)}\boldsymbol{u}^2(\boldsymbol{y}^1,\boldsymbol{y}^2), \text{ and,}\\ \boldsymbol{f}_2(\boldsymbol{y}^1,\boldsymbol{y}^2) &= \boldsymbol{g}_2 - \boldsymbol{V}_{\boldsymbol{r}^2(\boldsymbol{y}^2),\boldsymbol{r}^1(\boldsymbol{y}^1)}\boldsymbol{u}^1(\boldsymbol{y}^1,\boldsymbol{y}^2).\end{aligned}$$

Next, we approximate $\boldsymbol{f}_1$, and $\boldsymbol{f}_2$. To this end, we recall that the set of boundary traces of plane-waves (of a fixed wave-number and variable directions) are dense in $L^2(\gamma)$, where γ is the boundary of a bounded, simply connected Lipschitz domain, provided that the wavenumber is not a eigenvalue of the interior Laplace Dirichlet problem, see *e.g.* Section 3.4 of [14]. Standard arguments for open arcs (see, *e.g.* [41]) guarantee that we can extend this result to the scenario of γ being an open arc.

Being $L^2(\gamma)$ a dense subset of $\mathbb{W}^{\frac{1}{2}}(\gamma)$, one may claim the following: For each $\boldsymbol{y}^1, \boldsymbol{y}^2 \in \mathrm{U}$ and $\epsilon > 0$ there exist $L \in \mathbb{N}$ and

$$\left\{\alpha_1^\ell(\boldsymbol{y}^1,\boldsymbol{y}^2)\right\}_{\ell=1}^L \subset \mathbb{C}, \quad \left\{\beta_1^\ell(\boldsymbol{y}^1,\boldsymbol{y}^2)\right\}_{\ell=1}^L \subset \mathbb{C}, \quad \text{and} \quad \left\{\theta_1^\ell(\boldsymbol{y}^1,\boldsymbol{y}^2)\right\}_{\ell=1}^L \subset [0,2\pi), \tag{5.2}$$

such that

$$\left\| \boldsymbol{f}_1(\boldsymbol{y}^1,\boldsymbol{y}^2) - \sum_{\ell=1}^{L} \alpha_1^\ell \boldsymbol{e}_{(\theta_1^\ell)} g_{\theta_1^\ell,k_\mathrm{p}} \circ \boldsymbol{r}^1(\boldsymbol{y}^1) + \beta_1^\ell \boldsymbol{e}_{(\theta_1^\ell+\frac{\pi}{2})} g_{\theta_1^\ell,k_\mathrm{p}} \circ \boldsymbol{r}^1(\boldsymbol{y}^1) \right\|_{\mathbb{W}^{\frac{1}{2}}} < \epsilon,$$

and a equivalent result holds for $\boldsymbol{f}_2(\boldsymbol{y}_1,\boldsymbol{y}_2)$. We remark that the quantities in (5.2) depend continuously on the parametric inputs $\boldsymbol{y}^1, \boldsymbol{y}^2 \in \mathrm{U}$ and on $\epsilon > 0$. For $\boldsymbol{y}^1, \boldsymbol{y}^2 \in \mathrm{U}$, let us now define the collection of functions

$$\left\{\boldsymbol{v}_j^\ell(\boldsymbol{y}^1,\boldsymbol{y}^2)\right\}_{\ell=1}^L \subset \mathbb{T}^{-\frac{1}{2}}, \quad \text{and} \quad \left\{\boldsymbol{w}_j^\ell(\boldsymbol{y}^1,\boldsymbol{y}^2)\right\}_{\ell=1}^L \subset \mathbb{T}^{-\frac{1}{2}},$$

for $j = 1, 2$, as

$$\begin{aligned}\boldsymbol{V}_{\boldsymbol{r}^j(\boldsymbol{y}^j),\boldsymbol{r}^j(\boldsymbol{y}^j)}\boldsymbol{v}_j^\ell(\boldsymbol{y}^1,\boldsymbol{y}^2) &= \boldsymbol{e}_{(\theta_j^l)} g_{\theta_j^l,\kappa_\mathrm{p}} \circ \boldsymbol{r}^j(\boldsymbol{y}^j) \quad \text{and,}\\ \boldsymbol{V}_{\boldsymbol{r}^j(\boldsymbol{y}^j),\boldsymbol{r}^j(\boldsymbol{y}^j)}\boldsymbol{w}_j^\ell(\boldsymbol{y}^1,\boldsymbol{y}^2) &= \boldsymbol{e}_{(\theta_j^l+\frac{\pi}{2})} g_{\theta_j^l,\kappa_\mathrm{p}} \circ \boldsymbol{r}^j(\boldsymbol{y}^j),\end{aligned}$$

and their rotations by the angle $\phi_j^\ell(\boldsymbol{y}^1,\boldsymbol{y}^2) = \theta - \theta_j^\ell(\boldsymbol{y}^1,\boldsymbol{y}^2)$, denoted by

$$\widetilde{\boldsymbol{v}}_j^\ell(\boldsymbol{y}^1,\boldsymbol{y}^2) = \boldsymbol{R}_{\phi_j^\ell(\boldsymbol{y}^1,\boldsymbol{y}^2)}\boldsymbol{v}_j^\ell(\boldsymbol{y}^1,\boldsymbol{y}^2) \quad \text{and} \quad \widetilde{\boldsymbol{w}}_j^\ell(\boldsymbol{y}^1,\boldsymbol{y}^2) = \boldsymbol{R}_{\phi_j^\ell(\boldsymbol{y}^1,\boldsymbol{y}^2)}\boldsymbol{w}_j^\ell(\boldsymbol{y}^1,\boldsymbol{y}^2),$$

for $j = 1, 2$.

Given $\theta, \tilde{\theta} \in [0, 2\pi)$ one has $g_{\theta,\kappa}(\boldsymbol{R}_{\theta-\tilde{\theta}}\boldsymbol{x}) = g_{\tilde{\theta},\kappa}(\boldsymbol{x})$. Also, observe that $\boldsymbol{G}$ is invariant under translations, *i.e.* $\boldsymbol{G}(\boldsymbol{x}+\boldsymbol{d},\boldsymbol{y}+\boldsymbol{d}) = \boldsymbol{G}(\boldsymbol{x},\boldsymbol{y})$ for any $\boldsymbol{x},\boldsymbol{y},\boldsymbol{d} \in \mathbb{R}^2$. However, it is not invariant under rotations. Instead, the following holds $\boldsymbol{G}(\boldsymbol{R}_\theta\boldsymbol{x},\boldsymbol{R}_\theta\boldsymbol{y}) = \boldsymbol{R}_\theta\boldsymbol{G}(\boldsymbol{x},\boldsymbol{y})\boldsymbol{R}_\theta^\top$. These observations imply that

$$\begin{aligned}\boldsymbol{V}_{\widetilde{\boldsymbol{r}}^j(\boldsymbol{y}^j),\widetilde{\boldsymbol{r}}^j(\boldsymbol{y}^j)}\widetilde{\boldsymbol{v}}_j^\ell(\boldsymbol{y}^1,\boldsymbol{y}^2) &= \boldsymbol{e}_{(\theta)} g_{\theta,\kappa_\mathrm{p}} \circ \widetilde{\boldsymbol{r}}^j(\boldsymbol{y}^j) \quad \text{and}\\ \boldsymbol{V}_{\widetilde{\boldsymbol{r}}^j(\boldsymbol{y}^j),\widetilde{\boldsymbol{r}}^j(\boldsymbol{y}^j)}\widetilde{\boldsymbol{w}}_j^\ell(\boldsymbol{y}^1,\boldsymbol{y}^2) &= \boldsymbol{e}_{(\theta+\frac{\pi}{2})} g_{\theta,\kappa_\mathrm{p}} \circ \widetilde{\boldsymbol{r}}^j(\boldsymbol{y}^j),\end{aligned}$$

where $\widetilde{\boldsymbol{r}}^j(\boldsymbol{y}^j) = \boldsymbol{R}_{\phi_j^\ell}\boldsymbol{r}^j(\boldsymbol{y}^j)$, for $j = 1, 2$.

It follows from Assumption 5.3 we have that $\widetilde{\boldsymbol{r}}^j(\boldsymbol{y}^j)$ belongs to Σ. Consequently, $\widetilde{\boldsymbol{v}}_j^\ell, \widetilde{\boldsymbol{w}}_j^\ell$ are in the solution manifold of the single arc problem. In this setting, we obtain the following approximation result.

Proposition 5.5. *Let V be any closed subspace of $\mathbb{T}^{-\frac{1}{2}}$, and $\theta \in [0, 2\pi)$. Given $\epsilon > 0$ there exist $L \in \mathbb{N}$, $\{\theta_j^\ell\}_{\ell=1}^L \subset [0, 2\pi)$ and functions $\{\alpha_j^\ell(\boldsymbol{y}^1, \boldsymbol{y}^2)\}_{\ell=1}^L, \{\beta_j^\ell(\boldsymbol{y}^1, \boldsymbol{y}^2)\}_{\ell=1}^L \subset \mathbb{C}$, depending on the parametric inputs $\boldsymbol{y}^1, \boldsymbol{y}^2$, such that for $j = 1, 2$*

$$\begin{aligned}
&\left\|\boldsymbol{u}^j(\boldsymbol{y}^1, \boldsymbol{y}^2) - P_V \boldsymbol{u}^j(\boldsymbol{y}^1, \boldsymbol{y}^2)\right\|_{\mathbb{T}^{-\frac{1}{2}}} \\
&\qquad \lesssim \epsilon + \sum_{\ell=1}^{L} |\alpha_j^\ell(\boldsymbol{y}^1, \boldsymbol{y}^2)| \left(\left\|\widetilde{\boldsymbol{v}}_j^\ell(\boldsymbol{y}^1, \boldsymbol{y}^2) - P_V \widetilde{\boldsymbol{v}}_j^\ell(\boldsymbol{y}^1, \boldsymbol{y}^2)\right\|_{\mathbb{T}^{-\frac{1}{2}}} + \mathcal{E}\big(\mathcal{M}^\theta, V\big)\right) \\
&\qquad\quad + \sum_{\ell=1}^{L} |\beta_j^\ell(\boldsymbol{y}^1, \boldsymbol{y}^2)| \left(\left\|\widetilde{\boldsymbol{w}}_j^\ell(\boldsymbol{y}^1, \boldsymbol{y}^2) - P_V \widetilde{\boldsymbol{w}}_j^\ell(\boldsymbol{y}^1, \boldsymbol{y}^2)\right\|_{\mathbb{T}^{-\frac{1}{2}}} + \mathcal{E}\big(\mathcal{M}^{\theta+\frac{\pi}{2}}, V\big)\right),
\end{aligned}$$

where

$$\mathcal{E}(\mathcal{M}, V) = \sup_{\substack{\theta \in [0, 2\pi) \\ \boldsymbol{x} \in P_V(\mathcal{M})}} \|\boldsymbol{R}_\theta \boldsymbol{x} - P_V \boldsymbol{R}_\theta \boldsymbol{x}\|_{\mathbb{T}^{-\frac{1}{2}}} \tag{5.4}$$

measures how well rotations of the set $\mathcal{M}$ can be approximated by the space V.

Proof. For $\boldsymbol{y}^j \in \mathrm{U}$, with $j = 1, 2$ observe that

$$\begin{aligned}
\left\|\boldsymbol{u}^j(\boldsymbol{y}^1, \boldsymbol{y}^2) - P_V \boldsymbol{u}^j(\boldsymbol{y}^1, \boldsymbol{y}^2)\right\|_{\mathbb{T}^{-\frac{1}{2}}} &\leq 2 \left\| \boldsymbol{u}^j(\boldsymbol{y}^1, \boldsymbol{y}^2) - \sum_{\ell=1}^{L} \alpha_j^\ell(\boldsymbol{y}^1, \boldsymbol{y}^2) \boldsymbol{v}_j^\ell + \beta_j^\ell(\boldsymbol{y}^1, \boldsymbol{y}^2) \boldsymbol{w}_j^\ell \right\|_{\mathbb{T}^{-\frac{1}{2}}} \\
&\quad + \sum_{\ell=1}^{L} |\alpha_j^\ell(\boldsymbol{y}^1, \boldsymbol{y}^2)| \left\|\boldsymbol{v}_j^\ell(\boldsymbol{y}^1, \boldsymbol{y}^2) - P_V \boldsymbol{v}_j^\ell(\boldsymbol{y}^1, \boldsymbol{y}^2)\right\|_{\mathbb{T}^{-\frac{1}{2}}} \\
&\quad + \sum_{\ell=1}^{L} |\beta_j^\ell(\boldsymbol{y}^1, \boldsymbol{y}^2)| \left\|\boldsymbol{w}_j^\ell(\boldsymbol{y}^1, \boldsymbol{y}^2) - P_V \boldsymbol{w}_j^\ell(\boldsymbol{y}^1, \boldsymbol{y}^2)\right\|_{\mathbb{T}^{-\frac{1}{2}}}.
\end{aligned} \tag{5.5}$$

In the following, for economy of notation, we do not explicitly state the dependence upon the parametric variables $\boldsymbol{y}^1$ and $\boldsymbol{y}^2$. The first term on the right-hand side of (5.5) can be bounded using the well-possedness of the boundary integral formulation. Indeed, for $j = 1, 2$, one has

$$\begin{aligned}
\left\| \boldsymbol{u}^j - \sum_{\ell=1}^{L} \alpha_j^\ell \boldsymbol{v}_j^\ell + \beta_j^\ell \boldsymbol{w}_j^\ell \right\|_{\mathbb{T}^{-\frac{1}{2}}} &\lesssim \left\| \boldsymbol{V}_{\boldsymbol{r}^j, \boldsymbol{r}^j} \left(\boldsymbol{u}^j - \sum_{l=1}^{L} \alpha_j^\ell \boldsymbol{v}_j^\ell + \beta_j^\ell \boldsymbol{w}_j^\ell \right) \right\|_{\mathbb{W}^{\frac{1}{2}}} \\
&= \left\| \boldsymbol{f}_j - \sum_{l=1}^{L} \alpha_j^\ell \boldsymbol{e}_{\theta_j^\ell} g_{\theta_j^\ell, k_p} \circ \boldsymbol{r}^j + \beta_j^\ell \boldsymbol{e}_{\theta_j^\ell + \frac{\pi}{2}} g_{\theta_j^\ell, k_p} \circ \boldsymbol{r}^j \right\|_{\mathbb{W}^{\frac{1}{2}}} \\
&< \epsilon.
\end{aligned}$$

We bound the term $\left\|\boldsymbol{v}_j^\ell - P_V \boldsymbol{v}_j^\ell\right\|_{\mathbb{T}^{-\frac{1}{2}}}$, $\ell = 1, \ldots, L$, $j = 1, 2$, as all the remainder terms are similar. Using the definition of $\widetilde{\boldsymbol{v}}_j^l$ and the invariance of the 2-norm under rotations we have that

$$\begin{aligned}
\left\|\boldsymbol{v}_j^\ell - P_V \boldsymbol{v}_j^\ell\right\|_{\mathbb{T}^{-\frac{1}{2}}} &= \left\| \boldsymbol{R}_{\phi_j^\ell}^\top \widetilde{\boldsymbol{v}}_j^\ell - P_V \boldsymbol{R}_{\phi_j^\ell}^\top \widetilde{\boldsymbol{v}}_j^\ell \right\|_{\mathbb{T}^{-\frac{1}{2}}} \\
&\leq \left\|\widetilde{\boldsymbol{v}}_j^\ell - P_V \widetilde{\boldsymbol{v}}_j^\ell\right\|_{\mathbb{T}^{-\frac{1}{2}}} + \left\| \left(\boldsymbol{R}_{\phi_j^\ell}^\top P_V - P_V \boldsymbol{R}_{\phi_j^\ell}^\top \right) \widetilde{\boldsymbol{v}}_j^\ell \right\|_{\mathbb{T}^{-\frac{1}{2}}}.
\end{aligned}$$

In addition, we have

$$\begin{aligned}
\left\| \left(\boldsymbol{R}_{\phi_j^\ell}^\top P_V - P_V \boldsymbol{R}_{\phi_j^\ell}^\top \right) \widetilde{\boldsymbol{v}}_j^\ell \right\|_{\mathbb{T}^{-\frac{1}{2}}} &\leq \left\| \left(\boldsymbol{R}_{\phi_j^\ell}^\top P_V - P_V \boldsymbol{R}_{\phi_j^\ell}^\top P_V \right) \widetilde{\boldsymbol{v}}_j^\ell \right\|_{\mathbb{T}^{-\frac{1}{2}}} \\
&\quad + \left\| \left(P_V \boldsymbol{R}_{\phi_j^\ell}^\top P_V - P_V \boldsymbol{R}_{\phi_j^\ell}^\top \right) \widetilde{\boldsymbol{v}}_j^\ell \right\|_{\mathbb{T}^{-\frac{1}{2}}}.
\end{aligned}$$

Set $\boldsymbol{h} = P_V \widetilde{\boldsymbol{v}}_j^\ell$. Then, one has

$$\begin{aligned}\left\|\left(\boldsymbol{R}_{\phi_j^\ell}^\top P_V - P_V \boldsymbol{R}_{\phi_j^\ell}^\top P_V\right)\widetilde{\boldsymbol{v}}_j^\ell\right\|_{\mathbb{T}^{-\frac{1}{2}}} &= \left\|\left(\boldsymbol{R}_{\phi_j^\ell}^\top - P_V \boldsymbol{R}_{\phi_j^\ell}^\top\right)\boldsymbol{h}\right\|_{\mathbb{T}^{-\frac{1}{2}}} \\ &\leq \mathcal{E}(\mathcal{M}^\theta, V),\end{aligned}$$

where $\mathcal{E}(\mathcal{M}^\theta, V)$ is as in (5.4).

Using the continuity of $P_V \boldsymbol{R}_{\phi_j^\ell}^\top$ we obtain

$$\left\|\left(P_V \boldsymbol{R}_{\phi_j^\ell}^\top P_V - P_V \boldsymbol{R}_{\phi_j^\ell}^\top\right)\widetilde{\boldsymbol{v}}_j^\ell\right\|_{\mathbb{T}^{-\frac{1}{2}}} \leq \left\|P_V \widetilde{\boldsymbol{v}}_j^\ell - \widetilde{\boldsymbol{v}}_j^\ell\right\|_{\mathbb{T}^{-\frac{1}{2}}},$$

thus yielding

$$\left\|\left(\boldsymbol{R}_{\phi_j^\ell}^\top P_V - P_V \boldsymbol{R}_{\phi_j^\ell}^\top P_V\right)\widetilde{\boldsymbol{v}}_j^\ell\right\|_{\mathbb{T}^{-\frac{1}{2}}} \leq \mathcal{E}(\mathcal{M}^\theta, V) + \left\|P_V \widetilde{\boldsymbol{v}}_j^\ell - \widetilde{\boldsymbol{v}}_j^l\right\|_{\mathbb{T}^{-\frac{1}{2}}},$$

and finally replacing in the original bound of $\left\|\boldsymbol{v}_j^\ell - P_V \boldsymbol{v}_j^\ell\right\|_{\mathbb{T}^{-\frac{1}{2}}}$ we obtain the bound

$$\left\|\boldsymbol{v}_j^\ell - P_V \boldsymbol{v}_j^\ell\right\|_{\mathbb{T}^{-\frac{1}{2}}} \lesssim \left\|\widetilde{\boldsymbol{v}}_j^\ell - P_V \widetilde{\boldsymbol{v}}_j^\ell\right\|_{\mathbb{T}^{-\frac{1}{2}}} + \mathcal{E}\left(\mathcal{M}^\theta, V\right).$$

The bound for $\left\|\boldsymbol{w}_j^\ell - P_V \boldsymbol{w}_j^\ell\right\|_{\mathbb{T}^{-\frac{1}{2}}}$ follows from the same analysis, but replacing $\mathcal{M}^\theta$ by $\mathcal{M}^{\theta+\frac{\pi}{2}}$, as this is the solution manifold to which $\boldsymbol{w}_j^\ell$ belongs. Finally replacing in (5.5), we obtain the desire bound. □

Equipped with this we may now state the main result of this section concerning the convergence of the RB algorithm from for the multiple arc problem.

Theorem 5.6. *Let Assumptions 2.1 and 5.3 be satisfied for some $p \in (0,1)$. There exist $R_0, N_0 \in \mathbb{N}$, and $\varrho > 1$, such that for every $\epsilon > 0$ there exist $L(\epsilon) \in \mathbb{N}$, depending on $\epsilon > 0$, such that*

$$\varepsilon\left(V_R^{(\mathrm{rb})}\right) \lesssim M\left(\epsilon^2 + s^{-2\left(\frac{1}{p}-1\right)} + \varrho^{-2N} + LR^{-2\left(\frac{1}{p}-1\right)} + L\mathcal{E}^2\left(\mathcal{M}_N^\theta, V_R^{(\mathrm{rb})}\right) + L\mathcal{E}^2\left(\mathcal{M}_N^{\theta+\frac{\pi}{2}}, V_R^{(\mathrm{rb})}\right)\right)$$

where $\mathcal{E}(\mathcal{M}_N^\theta, V_R^{(\mathrm{rb})})$ and $\mathcal{E}(\mathcal{M}_N^{\theta+\frac{\pi}{2}}, V_R^{(\mathrm{rb})})$ are as in Proposition 5.5, and $\varepsilon(V_R^{(\mathrm{rb})})$ as in (5.1).

Proof. By using the same arguments of the analysis for a single arc we obtain the following bound

$$\begin{aligned}\varepsilon\left(V_R^{(\mathrm{rb})}\right) \lesssim\ & M\left(s^{-2\left(\frac{1}{p}-1\right)} + \varrho^{-2N}\right) \\ & + \sum_{j=1}^M \int_{\mathrm{U}^s} \cdots \int_{\mathrm{U}^s} \left\|\boldsymbol{u}_N^j\left(\boldsymbol{y}_{\{1:s\}}^1, \ldots, \boldsymbol{y}_{\{1:s\}}^M\right) - P_R^{(\mathrm{rb})} \boldsymbol{u}_N^j\left(\boldsymbol{y}_{\{1:s\}}^1, \ldots, \boldsymbol{y}_{\{1:s\}}^M\right)\right\|_{\mathbb{T}^{-\frac{1}{2}}}^2 \mathrm{d}\boldsymbol{y}^1 \ldots \mathrm{d}\boldsymbol{y}^M.\end{aligned}$$

An inspection of Proposition 5.5 reveals that the statement continues to be valid for the discrete counterpart of the multiple arc problem. Consequently, for any $\epsilon > 0$ there exist $L \in \mathbb{N}$ such that for $j = 1, \ldots, M$ it holds

$$\begin{aligned}&\left\|\boldsymbol{u}_N^j\left(\boldsymbol{y}_{\{1:s\}}^1, \ldots, \boldsymbol{y}_{\{1:s\}}^M\right) - P_R^{(\mathrm{rb})} \boldsymbol{u}_N^j\left(\boldsymbol{y}_{\{1:s\}}^1, \ldots, \boldsymbol{y}_{\{1:s\}}^M\right)\right\|_{\mathbb{T}^{-\frac{1}{2}}} \\ &\qquad \lesssim \epsilon + \sum_{\ell=1}^L |\alpha_j^\ell| \left(\left\|\widetilde{\boldsymbol{v}}_j^\ell - P_R^{(\mathrm{rb})} \widetilde{\boldsymbol{v}}_j^\ell\right\|_{\mathbb{T}^{-\frac{1}{2}}} + \mathcal{E}\left(\mathcal{M}_N^\theta, V_R^{(\mathrm{rb})}\right)\right) \\ &\qquad\quad + \sum_{\ell=1}^L |\beta_j^\ell| \left(\left\|\widetilde{\boldsymbol{w}}_j^\ell - P_R^{(\mathrm{rb})} \widetilde{\boldsymbol{w}}_j^\ell\right\|_{\mathbb{T}^{-\frac{1}{2}}} + \mathcal{E}\left(\mathcal{M}_N^{\theta+\frac{\pi}{2}}, V_R^{(\mathrm{rb})}\right)\right).\end{aligned} \tag{5.6}$$

We remark that in (5.6), just for economy of notation, we did not explicitly include the dependence upon the parametric variables $\boldsymbol{y}_{\{1:s\}}^1, \ldots, \boldsymbol{y}_{\{1:s\}}^M$ in the last two terms.

By Assumption 5.3 we have that $\widetilde{\boldsymbol{v}}_j^\ell$, and $\widetilde{\boldsymbol{w}}_j^\ell$ are elements of the discrete solution manifold. Arguing as in the case of a single arc, in particular as in items (iii) and (iv) of the results presented in Section 5.2.1, we have the following bounds

$$\left\|\widetilde{\boldsymbol{v}}_j^\ell\left(\boldsymbol{y}_{\{1:s\}}^1,\ldots,\boldsymbol{y}_{\{1:s\}}^M\right)-P_R^{(\mathrm{rb})}\widetilde{\boldsymbol{v}}_j^\ell\left(\boldsymbol{y}_{\{1:s\}}^1,\ldots,\boldsymbol{y}_{\{1:s\}}^M\right)\right\|_{\mathbb{T}^{-\frac{1}{2}}}\lesssim R^{-\left(\frac{1}{p}-1\right)}\quad\text{and}$$
$$\left\|\widetilde{\boldsymbol{w}}_j^\ell\left(\boldsymbol{y}_{\{1:s\}}^1,\ldots,\boldsymbol{y}_{\{1:s\}}^M\right)-P_R^{(\mathrm{rb})}\widetilde{\boldsymbol{w}}_j^\ell\left(\boldsymbol{y}_{\{1:s\}}^1,\ldots,\boldsymbol{y}_{\{1:s\}}^M\right)\right\|_{\mathbb{T}^{-\frac{1}{2}}}\lesssim R^{-\left(\frac{1}{p}-1\right)}.$$

Finally, it follows from a compactness argument and the continuity of the functions α_j^ℓ and β_j^ℓ for a given $\epsilon>0$ the corresponding value of L can be selected such that do not depend of the parameters $\boldsymbol{y}_{\{1:s\}}^1,\ldots,\boldsymbol{y}_{\{1:s\}}^M$, and that α_j^ℓ, and β_j^ℓ can also be bounded independently of the parameters thus yielding the stated result. □

Various remarks are in place regarding the convergence of the multiple arcs problem. First, the presence of the term $\mathcal{E}(\mathcal{M}_N^\theta,V_R^{(\mathrm{rb})})$ in Proposition 5.5 is a result of the lack of invariance under rotation of the fundamental solution of the elastic wave problem. For acoustic formulation or EFIE formulation for Maxwell equation this term does not appear. In addition, the value of L and ϵ of Theorem 5.6 are obviously related, as $\epsilon>0$ can be interpreted as the convergence rate of the approximation by plane waves of a particular solution of the Navier equation. In particular for the Helmholtz equation the relation is well understood, see *e.g.* [36]. Furthermore, if we can show that $\sum_{\ell=1}^\infty|\alpha_j^\ell|$, and $\sum_{\ell=1}^\infty|\beta_j^\ell|$ are bounded for every $\boldsymbol{y}_{\{1:s\}}^1,\ldots,\boldsymbol{y}_{\{1:s\}}^M$, then the bound of Theorem 5.6 would not depend explicitly on L.

6. Numerical results

We present numerical experiments illustrating the performance of the reduced order algorithm for the multiple arcs problem.

6.1. Fixed number of arcs

We consider $M=16$ open arcs enclosed in the two-dimensional box $[-10,10]\times[-10,10]$. In addition, we consider the setting described in Section 2.3 with parameters $r_{\min}=0.56$, $r_{\max}=0.93$, $d_{\min}=5$, $d_{\max}=21$, and perturbations terms in (4.11a) and (4.11b) of the form

$$\sum_{n=1}^{3}c_n\sum_{p=1}^{2}\left(\cos((n-1)t)\boldsymbol{e}_p y_{6(p-1)+2n}+\sin(nt)\boldsymbol{e}_p y_{6(p-1)+2n-1}\right),\quad \boldsymbol{y}\in\mathrm{U}^s,\tag{6.1}$$

with dimension truncation $s=12$ and $c_n=n^{-\frac{5}{2}}$. A realization of this setting is presented in Figure 1. We consider the elastic-wave scattering operator with parameters $\omega=10$, $\lambda=2$, $\mu=1$.

We investigate the convergence of the high-fidelity solver described in Section 3.2 for this configuration. To this end, we consider 512 geometry realization and take the average error in the $\mathbb{T}^0$-norm. These results are presented in Figure 2.

Based on the errors achieved by the high-fidelity solver, for further results related to this test case we fix $N=40$, unless otherwise specified.

Now we analyze whether the multiple arc problem is amenable for complexity reduction. We consider a number of snapshots and inspect the singular values of the snapshot matrix. These are presented in Figure 3. We observe that while the singular values decay exponentially, we are not able to achieve relative small tolerances. Consequently, this configuration is not directly amenable for reduction.

Hence, as pointed out in Section 4.2, we have two key issues.

(1) The dimension of the perturbation parameter is $12\times16=192$, and many (at least twice the total number of arcs) share the same importance. This is the main reason as to why is hard to find a suitable reduced basis for the multiple arc problem.

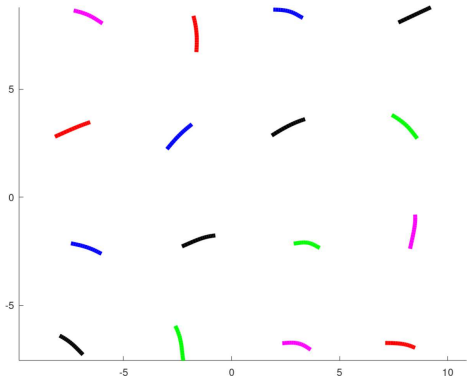

FIGURE 1. Geometry realization of 16 open arcs with parametrically defined perturbations as described in (6.1).

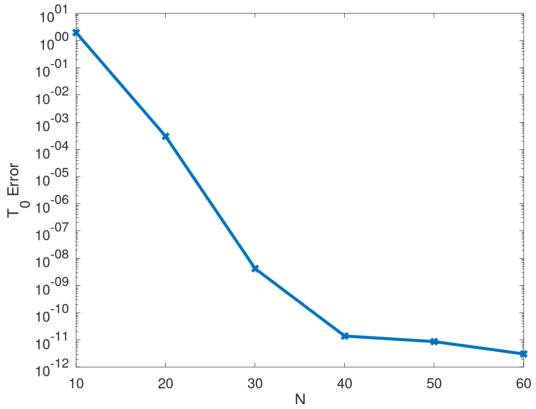

FIGURE 2. Convergence of the high-fidelity solver with respect to an overkill solution obtained with $N = 100$, for the 16 arcs problems, with $\omega = 10, \lambda = 2, \mu = 1$, and geometry perturbations as in (6.1), errors computed as the average over 512 realizations of the geometry.

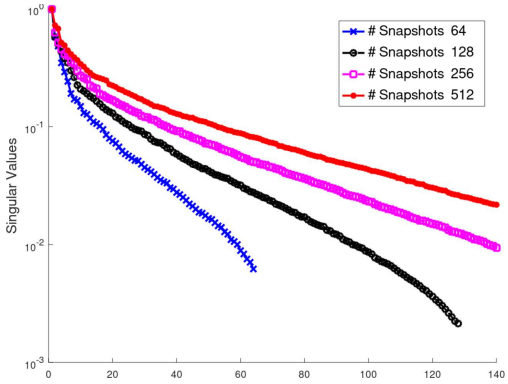

FIGURE 3. Singular values of the snapshot matrix of the multiple arc problem (16 arcs) scaled by the magnitude of the first singular-value, width $N = 70$ as parameter for the high-fidelity solver.

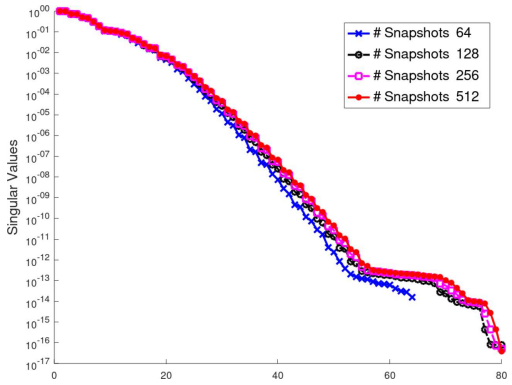

FIGURE 4. Singular values for a single arc, scaled by the magnitude of the first singular-value, with $N = 100$ as discretization parameter for the high-fidelity solver.

(2) Even if we could find good basis for the full problem, the cost of constructing this basis can be extremely high, as we would require to solve a large number of full-order problems.

Next we study whether the single arc problem is suitable for reduction. As explained in Section 4.3, we consider a parametrization of the arc that includes the effects of the position, orientation and length as variables determined by the random parameters, as well as perturbations of the form (6.1). These results are presented in Figure 4. As opposed to the multiple arc problem, for a single arc we can achieve much smaller relative singular values.

It remains to elucidate if the reduced basis for the single arc problem performs accurately for the multiple arc problem. The following results illustrate that this is indeed the case.

We investigate the convergence of the interpolation procedure described in Section 4.3. We are interested in the evolution of the relative errors as the number of iterations of the empirical interpolation method (*i.e.* Algorithm 1) increases. Observe that the fundamental solution is a 2×2 matrix. Therefore, we need to compute four scalar interpolations. However, the pair of diagonal terms exhibits a similar behavior and so does the pair of off-diagonal terms. Thus, we only show results for the entries $(1, 1)$ and $(1, 2)$. We also recall that according to Remark 3.4, for the self-interactions we have to interpolate two type of functions: the regular-part, which for the sake of simplicity is referred to as Reg-Part, and the J-part. The corresponding results are presented in Figure 5.

We make the following remarks concerning these results:

(1) The error appears to decrease exponentially, as the slope of the error curve is approximately constant.
(2) The cross-interaction matrices need a higher number of terms to achieve the same level of accuracy. This should be expected as the cross-interaction term is of higher dimension as it depends on two parametrically defined arcs

We present the errors of the reduced basis method for the multiple arc problem. We recall that according to Sections 4.1 and 4.3 the accuracy of the reduced basis method depends of two parameters: ϵ_{svd} that determines the number of basis and ϵ_{eim} the tolerance used to construct the interpolation of the corresponding functions. In Figure 6 we present the average error of 56 test cases[6] depending of the number of reduced basis used R, which is determined by ϵ_{svd} and ϵ_{eim}. The solution of the respective linear system is computed using the preconditioned GMRES.

To further illustrate the performance of the method, in Table 1 we include some extra information regarding these test cases, such as the tolerances used and the execution times: Times-RB (solution time for the reduced

[6]These 56 configurations are not part of the snapshots set.

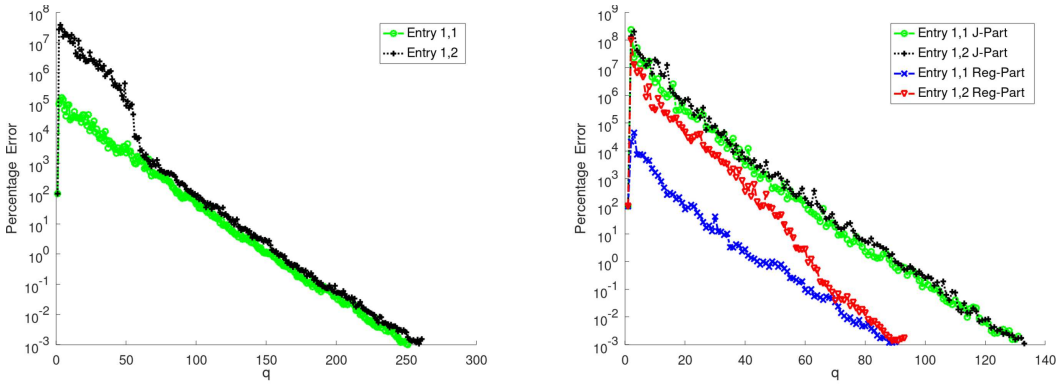

(a) (b)

FIGURE 5. Percentage error of the interpolation procedure for the different blocks of the fundamental solution with respect to the number of iterations of Algorithm 1, for the 16 arcs problems, with $\omega = 10, \lambda = 2, \mu = 1$, and geometry perturbations as in (6.1). (a) Cross-interactions. (b) Self-interactions.

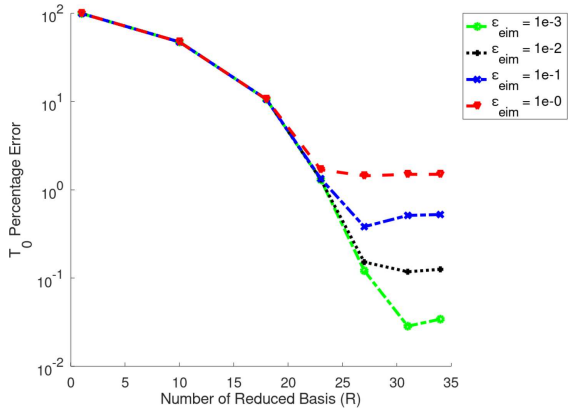

FIGURE 6. Mean value of the errors of the reduced basis method for the 16 arcs problems, with $\omega = 10, \lambda = 2, \mu = 1$, and geometry perturbations as in (6.1).

basis), Times-HF (solution time for the high-fidelity), and the values of R (number of reduced basis) and Q (number of terms in the interpolation), for the latter we show a weighted mean value, as the value differs for each of the four entries of the fundamental solution, and also if it correspond to a cross or self-interaction. The associated weights are $\frac{M^2-M}{M^2}$, for the cross-interactions, and $\frac{M}{M^2}$, for the self-interactions.

6.2. Increasing number of arcs

We again consider the problem with $\omega = 10$, $\lambda = 2$, $\mu = 1$, and perturbations of the form (6.1), but with $c_n = \frac{\min(1,r_{\max})}{n^{2.5}}$. The arcs are again positioned in $[-10, 10] \times [-10, 10]$, but the number of arcs, as well as the global parameters $r_{\min}, r_{\max}, d_{\min}, d_{\max}$, are variable. In particular, we consider different number of arcs, from 36 to 1024, and we adapt the global geometry parameters to ensure that no self crossing occurs. We illustrate some geometry realizations in Figure 7.

TABLE 1. Convergence results for the high-fidelity solver as well as the reduced basis model. The parameters are 16 arcs $\omega = 10, \lambda = 2, \mu = 1$, and geometry perturbations as in (6.1).

ϵ_{svd}	R	ϵ_{eim}	Mean of Q	Time-RB	Time-HF	Percentage error
1e−6	34	1e−3	245	3.1 s	6 s	3.4e−2
1e−6	34	1e−1	179	2 s	6 s	5e−1
1e−3	23	1e−3	245	2.8 s	6 s	1.3
1e−3	23	1e−1	179	1.8 s	6 s	1.3
1e−1	10	1e−3	245	2.5 s	6 s	47
1e−1	10	1e−1	179	1.5 s	6 s	47

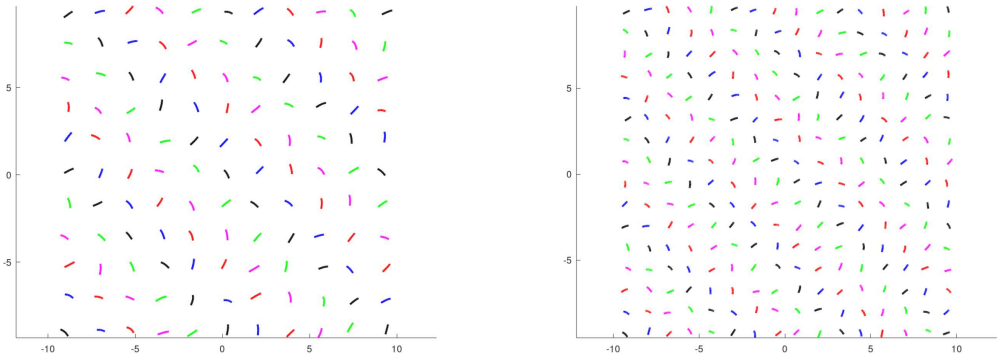

(a) (b)

FIGURE 7. Geometry realizations. (a) 121 Arcs. (b) 256 Arcs.

Observe that the size of the arcs decreases as the number of arcs increases. This is equivalent to reduce the frequency as the number of arcs increases. Consequently, the corresponding single arc problem used for constructing the reduced space becomes computationally simpler as we increase the number of arcs.

In some of the cases considered in this section (529 and 1024 arcs) it is impossible (given the memory constraints[7]) to obtain the solutions using the high-fidelity solver. We consider an *a posteriori* estimation of the error to illustrate the performance of the method. To this end, we define the relative residual as,

$$\text{res} = \sum_{k=1}^{M} \frac{\| \sum_{j=1}^{M} \mathbb{A}_{k,j} \mathbb{V}_R^{(\text{rb})} \boldsymbol{a}_R^{(\text{rb}),j} - \boldsymbol{g}_k \|^2}{\| \boldsymbol{g}_k \|^2}.$$

The results are presented in Table 2.

7. CONCLUDING REMARKS

In this work, we present and analyze a reduced basis algorithm for the elastic scattering by multiple arcs in two space dimensions. The key insight of the method, which as previously mentioned follows [23], consists first in finding a reduced space for a single shape-parametric, and then use this as a building block for the construction of a reduced space for the multiple open arcs problem. Among the advantages of this method, we highlight that once the reduced basis has been constructed and stored in the offline phase, one can use this reduced space for

[7]All the experiments were performed on a desktop computer I7-4770 with 32 GB of RAM.

TABLE 2. Results for number of arcs (M), with $N = 70$ for the high-fidelity solver, $\epsilon_{\text{svd}} = \epsilon_{\text{eim}} = 10^{-3}$. Parameters are $\omega = 10, \lambda = 2, \mu = 1$, and geometry perturbations are as in (6.1).

M	R	Mean Q	Time-RB	Time-HF	Percentage error	Percentage residual
36	22	175	9 s	90 s	0.07	0.01
64	20	140	21 s	290 s	0.05	0.007
121	18	112	70 s	479 s	0.04	0.006
256	16	88.8	311 s	4640 s	0.04	0.003
529	14	70	1820 s	–	–	0.005
1024	14	60	11 800 s	–	–	0.001

the computation solution of different multiple arcs configuration, possibly with different number of arcs, in the online phase of the reduced basis method. Furthermore, based on our previous work [37], we present a complete analysis of the method. In particular, in our analysis, we provide an argument as to why the reduced basis for the single arc serves for the multiple arcs problem. Even though we have presented a complete description for the multiple arcs problem equipped with Dirichlet boundary conditions, the exact same analysis can be extended to the same problem equipped with Neumann boundary conditions. This would lead to a boundary integral formulation characterized by the presence of hypersingular BIOs. Future work comprises the extension of this work and analysis to acoustic and elastic scattering by multiple objects in three dimensions, and the construction of neural network-based surrogates for the approximation of the corresponding parameter-to-solution map as in [27].

FUNDING

This work was funded by the ANID grant Fondecyt Iniciación No. 11230248.

REFERENCES

[1] S. Andrieux and A.B. Abda, Identification of planar cracks by complete overdetermined data: inversion formulae. *Inverse Prob.* **12** (1996) 553.

[2] K.E. Atkinson and I.H. Sloan, The numerical solution of first-kind logarithmic-kernel integral equations on smooth open arcs. *Math. Comput.* **56** (1991) 119–139.

[3] P. Binev, A. Cohen, W. Dahmen, R. DeVore, G. Petrova and P. Wojtaszczyk, Convergence rates for greedy algorithms in reduced basis methods. *SIAM J. Math. Anal.* **43** (2011) 1457–1472.

[4] O.P. Bruno, L. Xu and T. Yin, Weighted integral solvers for elastic scattering by open arcs in two dimensions. *Int. J. Numer. Methods Eng.* **122** (2021) 2733–2750.

[5] A. Buffa, Y. Maday, A.T. Patera, C. Prud'homme and G. Turinici, A priori convergence of the greedy algorithm for the parametrized reduced basis method. *ESAIM:M2AN* **46** (2012) 595–603.

[6] T. Bui-Thanh, K. Willcox and O. Ghattas, Model reduction for large-scale systems with high-dimensional parametric input space. *SIAM J. Sci. Comput.* **30** (2008) 3270–3288.

[7] R. Chapko, R. Kress and L. Mönch, On the numerical solution of a hypersingular integral equation for elastic scattering from a planar crack. *IMA J. Numer. Anal.* **20** (2000) 601–619.

[8] P. Chen and C. Schwab, Sparse-grid, reduced-basis Bayesian inversion. *Comput. Methods Appl. Mech. Eng.* **297** (2015) 84–115.

[9] P. Chen and C. Schwab, Adaptive sparse grid model order reduction for fast Bayesian estimation and inversion, in Sparse Grids and Applications-Stuttgart 2014. Springer (2016) 1–27.

[10] P. Chen and C. Schwab, Sparse-grid, reduced-basis Bayesian inversion: nonaffine-parametric nonlinear equations. *J. Comput. Phys.* **316** (2016) 470–503.

[11] A. Chkifa, A. Cohen and C. Schwab, Breaking the curse of dimensionality in sparse polynomial approximation of parametric PDEs. *J. Math. Pures Appl.* **103** (2015) 400–428.

[12] A. Cohen and R. DeVore, Approximation of high-dimensional parametric PDEs. *Acta Numer.* **24** (2015) 1–159.

[13] A. Cohen and R. DeVore, Kolmogorov widths under holomorphic mappings. *IMA J. Numer. Anal.* **36** (2016) 1–12.
[14] D.L. Colton, R. Kress and R. Kress, Inverse Acoustic and Electromagnetic Scattering Theory. Vol. 93. Springer (1998).
[15] M. Dalla Riva, J. Morais and P. Musolino, A family of fundamental solutions of elliptic partial differential operators with quaternion constant coefficients. *Math. Methods Appl. Sci.* **36** (2013) 1569–1582.
[16] M. Dalla Riva, P. Luzzini and P. Musolino, Multi-parameter analysis of the obstacle scattering problem. *Inverse Prob.* **38** (2022) 055004.
[17] M. Dalla Riva, P. Luzzini and P. Musolino, Shape analyticity and singular perturbations for layer potential operators. *ESAIM:M2AN* **56** (2022) 1889–1910.
[18] R. DeVore, G. Petrova and P. Wojtaszczyk, Greedy algorithms for reduced bases in Banach spaces. *Constr. Approx.* **37** (2013) 455–466.
[19] J. Dick, F.Y. Kuo, Q.T. Le Gia, D. Nuyens and C. Schwab, Higher order QMC Petrov–Galerkin discretization for affine parametric operator equations with random field inputs. *SIAM J. Numer. Anal.* **52** (2014) 2676–2702.
[20] J. Dick, Q.T. Le Gia and C. Schwab, Higher order quasi–Monte Carlo integration for holomorphic, parametric operator equations. *SIAM/ASA J. Uncertain. Quantif.* **4** (2016) 48–79.
[21] J. Dick, R.N. Gantner, Q.T.L. Gia and C. Schwab, Higher order quasi-Monte Carlo integration for Bayesian estimation. *Comput. Math. Appl.* **77** (2019) 144–172.
[22] J. Dölz and F. Henríquez, Parametric shape holomorphy of boundary integral operators with applications. *SIAM J. Math.* **56** (2024) 6731–6767.
[23] M. Ganesh, J.S. Hesthaven and B. Stamm, A reduced basis method for electromagnetic scattering by multiple particles in three dimensions. *J. Comput. Phys.* **231** (2012) 7756–7779.
[24] J.H. Halton, On the efficiency of certain quasi-random sequences of points in evaluating multi-dimensional integrals. *Numer. Math.* **2** (1960) 84–90.
[25] F. Henriquez, *Shape uncertainty quantification in acoustic scattering*. Ph.D. thesis, ETH Zurich (2021).
[26] F. Henríquez and C. Schwab, Shape holomorphy of the Calderón projector for the Laplacian in $\mathbb{R}^2$. *Integral Equ. Oper. Theory* **93** (2021) 43.
[27] J.S. Hesthaven and S. Ubbiali, Non-intrusive reduced order modeling of nonlinear problems using neural networks. *J. Comput. Phys.* **363** (2018) 55–78.
[28] J.S. Hesthaven, B. Stamm and S. Zhang, Efficient greedy algorithms for high-dimensional parameter spaces with applications to empirical interpolation and reduced basis methods. *ESAIM:M2AN* **48** (2014) 259–283.
[29] J.S. Hesthaven, G. Rozza and B. Stamm, Certified Reduced Basis Methods for Parametrized Partial Differential Equations. Vol. 590. Springer (2016).
[30] C. Jerez-Hanckes and J. Pinto, High-order Galerkin method for Helmholtz and Laplace problems on multiple open arcs. *ESAIM:M2AN* **54** (2020) 1975–2009.
[31] C. Jerez-Hanckes, J. Pinto and T. Yin, Spectral galerkin method for solving elastic wave scattering problems with multiple open arcs. *Commun. Math. Sci.* **22** (2024) 1839–1862.
[32] R. Kress, Inverse elastic scattering from a crack. *Inverse Prob.* **12** (1996) 667.
[33] Y. Liang, H. Lee, S. Lim, W. Lin, K. Lee and C. Wu, Proper orthogonal decomposition and its applications – Part I: theory. *J. Sound Vib.* **252** (2002) 527–544.
[34] Y. Maday, A.T. Patera and G. Turinici, A priori convergence theory for reduced-basis approximations of single-parameter elliptic partial differential equations. *J. Sci. Comput.* **17** (2002) 437–446.
[35] W. McLean, Strongly Elliptic Systems and Boundary Integral Equations. Cambridge University Press (2000).
[36] A. Moiola, R. Hiptmair and I. Perugia, Plane wave approximation of homogeneous helmholtz solutions. *Z. Angew. Math. Phys.* **62** (2011) 809–837.
[37] J. Pinto, F. Henríquez and C. Jerez-Hanckes, Shape holomorphy of boundary integral operators on multiple open arcs. *J. Fourier Anal. Appl.* **30** (2024) 14.
[38] C. Prud'Homme, D.V. Rovas, K. Veroy, L. Machiels, Y. Maday, A.T. Patera and G. Turinici, Reliable real-time solution of parametrized partial differential equations: reduced-basis output bound methods. *J. Fluids Eng.* **124** (2002) 70–80.
[39] A. Quarteroni, A. Manzoni and F. Negri, Reduced Basis Methods for Partial Differential Equations: An Introduction. Vol. 92. Springer (2015).
[40] G. Rozza, Fundamentals of reduced basis method for problems governed by parametrized PDEs and applications, in Separated Representations and PGD-Based Model Reduction: Fundamentals and Applications. Springer (2014) 153–227.

[41] S.A. Sauter and C. Schwab, Boundary Element Methods. Vol. 39 of *Springer Series in Computational Mathematics* (2011).
[42] C. Schillings and C. Schwab, Sparse, adaptive Smolyak quadratures for Bayesian inverse problems. *Inverse Prob.* **29** (2013) 065011.
[43] E.P. Stephan and W.L. Wendland, An augmented Galerkin procedure for the boundary integral method applied to two-dimensional screen and crack problems. *Appl. Anal.* **18** (1984) 183–219.
[44] J. Zech and C. Schwab, Convergence rates of high dimensional Smolyak quadrature. *ESAIM:M2AN* **54** (2020) 1259–1307.